Available online at www.sciencedirect.com
SCIENCE DIRECT
Coordination Chemistry Reviews 250 (2006) 1530–1561
COORDINATION CHEMISTRY REVIEWS
www.elsevier.com/locate/ccr

Review

Novel families of phthalocyanine-like macrocycles—Porphyrazines with annulated strongly electron-withdrawing 1,2,5-thia/selenodiazole rings

Maria Pia Donzello [a], Claudio Ercolani [a,*], Pavel A. Stuzhin [b,**]

[a] *Dipartimento di Chimica, Università degli Studi di Roma "La Sapienza", P. le A. Moro 5, Roma I-00185, Italy*
[b] *Department of Organic Chemistry, Ivanovo State University of Chemical Technology, Friedrich Engels Pr-t 7, Ivanovo RF-153460, Russia*

Received 31 October 2005; accepted 8 February 2006
Available online 6 March 2006

Contents

Abstract

Tetrakis(thiadiazole)porphyrazines and tetrakis(selenodiazole)porphyrazines, first described in the years 1998–2001, have later attracted the attention of different scientific groups in the world. Since the beginning and in the most recent times, a number of aspects concerning their relevance as phthalocyanine-like macrocycles, their distinct structural, electronic and UV–visible spectroscopic features, and electrochemical behavior have brought to knowledge the important role played by the externally annulated electron-withdrawing thia- and selenodiazole rings. Much has been learned about the acid–base properties of the new macrocycles, their facile electron uptake and negative charge redistribution capability within the entire macrocyclic framework. Further work has been directed to the synthesis and characterization of several low-symmetry species carrying peripherally annulated benzene or substituted benzene rings and thia- or selenodiazole rings and the structural and electronic effects caused by the progressive annulation of the heterocyclic rings in a basic phthalocyanine structure has been examined. Deselenation processes at the annulated selenodiazole rings in symmetrical and low-symmetry macrocycles and the formation of vicinal diamino functionalities have allowed diversified derivatization procedures with formation of new porphyrazine macrocycles by ring reclosure or designed external sites for exocyclic metalation in dinuclear species.

Keywords: Annulated porphyrazines; 1,2,5-Thia/selenodiazole; Synthesis; Structure; Spectroscopy; Electrochemistry; Acid–base properties

* Corresponding author. Tel.: +39 06 4991 3330; fax: +36 06 490324.
** Corresponding author. Tel.: +07 4932 477765; fax: +07 4932 335628.
E-mail addresses: claudio.ercolani@uniromal.it (C. Ercolani), stuzhin@isuct.ru (P.A. Stuzhin).

0010-8545/$ – see front matter © 2006 Elsevier B.V. All rights reserved.
doi:10.1016/j.ccr.2006.02.009

1. Introduction

Porphyrins and porphyrazines, the two main classes of tetrapyrrolic macrocycles, differ basically as the porphyrins are formally derived from the porphine molecule ([PH_2], Chart 1), whereas porphyrazines are constitutionally tetraazaanalogues of porphyrins since they have a porphyrazine-type central core with N atoms bridging the pyrrole rings instead of the CH groups present in the porphine and porphyrin skeleton ([PzH_2], Chart 1). Porphyrins are either naturally occurring molecular systems or original synthetic products, whereas porphyrazines derive exclusively from synthetic laboratory work. The best known and most widely studied class of porphyrazines are the phthalocyanines (tetrabenzoporphyrazines; exemplified in Chart 2 as [PcM] with Pc = phthalocyaninato dianion, $C_{32}H_{16}N_8^{2-}$, and M = bivalent non-transition or first-row transition metal ion). For several decades, since their discovery in the 1920s and the pioneering work by Linstead et al. in the 1930s [1], innumerable studies on [PcM] species and their analogues with different central metal ions and substituents on the external benzene rings have seen this class of porphyrazine macrocycles to attract scientists in a privileged fashion [2,3], whilst porphyrazines in general were only scarcely investigated. The physicochemical properties of the porphyrazine macrocycles certainly are basically dependent on the prerogatives of the central tetrapyrrolic core, but they are also modulated significantly, in terms of structural and electronic features, coordinative and chemical properties and general physicochemical behavior, by the incorporated central metal, as well as by the peripheral substituents or annulated aromatic rings.

In recent times, porphyrazines have gained more attention. Recently, a number of non-annulated β-substituted porphyrazines ([R_8PzM], Chart 2), often implying exocyclic coordination and formation of multinuclear species, have been prepared and characterized by Barrett, Hoffman and co-workers and the main results of this relevant work has been nicely reviewed [4]. An area of further expansion of new porphyrazine macrocycles can be that directed to the synthesis of new phthalocyanine-like macrocycles carrying heterocyclic rings directly annulated to the porphyrazine core, opening a route to new forms of investigation and promising potential practical applications. Although the inital attempts were made in the 1930s by Linstead to obtain phthalocyanine analogs in which the annulated

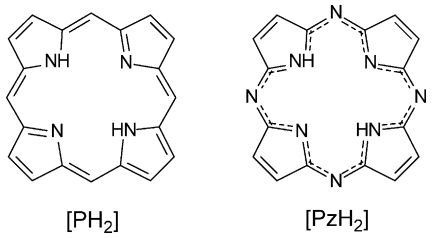

Chart 1. Porphine [PH_2] and porphyrazine [PzH_2].

benzene rings were substituted by five-membered aromatic heterocycles [5,6], since then only thiophene derivatives have been described in some detail [7–10]. In the last two to three decades, mainly porphyrazine systems carrying externally annulated six-membered pyridine and pyrazine rings have been reported [11]. A fairly complete overview on the porphyrazine macrocycles bearing annulated heterocyclic five-, six-, and seven-membered rings has recently been published by two of us [12].

Around the year 2000, two novel families of porphyrazine macrocycles were reported by Ercolani and co-workers [13–17]—the tetrakis(thia/selenodiazole)porphyrazines, [TTDPzM] and [TSeDPzM] (Chart 2; M = $2H^I$, $Mg^{II}(H_2O)$, Mn^{II}, Fe^{II}, Co^{II}, Ni^{II}, Cu^{II}, Zn^{II}). These new macrocycles, entering the class of porphyrazines (hereafter often referred to as "S- and "Se-porphyrazines") isolated as stable solid materials, are characterized by the presence of four heterocyclic five-membered rings, namely 1,2,5-thiadiazole and 1,2,5-selenodiazole (simplified hereafter as thia- and selenodiazole), annulated to the pyrrole rings of the porphyrazine core. Undoubtedly, these S- and Se-containing porphyrazines [14–17] are the type of macrocycles which structurally closely recall the phthalocyanine molecular framework and share with the phthalocyanine ring important properties like low solubility, stability, sublimability (S-compounds) and comparable chromophoric character, showing intense absorptions in the Soret and Q band regions. Nevertheless, they show distinct electronic features, physicochemical behavior and reactivity, due to the peripherally present strongly electron-withdrawing N–S–N and N–Se–N moieties. As will shortly be illustrated in the present work, the electron deficiency of the thia/selenodiazole rings, contiguous to the porphyrazine core in these novel series of macrocycles as well as in their parent low-symmetry species, strongly influences the

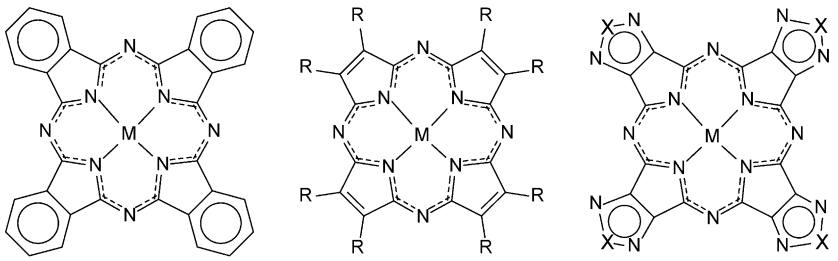

Chart 2.

σ/π electronic distribution within the entire highly π-conjugated molecular system. The effects are clearly seen with regard to the acidity strength manifested by the central NH groups in the unmetalated macrocycles [TTDPzH$_2$] and [TSeDPzH$_2$] and by the tendency shown by their metal complexes to expand their coordination number through axial ligation. The UV/vis solution spectra are quite informative as to the level of electron deficiency present in these type of macrocycles and comparison with the data on phthalocyanines adequately illustrates this aspect. Moreover, the presence in the new macrocycles of peripheral N, and soft S and Se atoms, rich of electrons, was seen [14–17] as an important requisite able to determine new forms of intermolecular contacts in the condensed phase, as indeed widely demonstrated by X-ray structural information now available, opening new perspectives for solid state investigations.

Following the initial studies [14–17], whilst parallel our work was extended to other new classes of porphyrazine macrocycles carrying externally annulated electron-withdrawing seven-membered diazepine [18] and six-membered dipyridinopyrazine fragments [19], the most recent years have seen the present series of "S- and "Se-porphyrazines" to become the object of growing interest and new related symmetrical and low-symmetry species have been prepared and investigated by the first group operative in this area [20–26] and by other authors [27–32]. The results obtained have provided more insight to and better understanding of the main structural and electronic features of this kind of "S- and "Se-porphyrazines" so far brought to knowledge, an important aspect in view of an extension of the work in differently targeted areas of research and applications. The purpose of the present work is to provide a concise overall view of the most significant results obtained on these two novel classes of S/Se containing porphyrazine macrocycles, whilst making previous fragmentarily exposed material [12,33,34] more updated and better accessible to the readers.

2. Synthetic aspects

The dicyano compounds **1** and **2** (Scheme 1), which can be easily obtained in a high yield by treatment of the inexpensive and commercially available diaminomaleodinitrile (DAMN) with $SOCl_2$ or SeO_2, respectively [14,16], are the key precursors for the preparation of the "S- and "Se-porphyrazines".

2.1. Symmetrical tetrakis(thia/selenodiazole)porphyrazines

Template macrocyclization of **1** or **2** occurs smoothly in the presence of Mg^{II}-propylate or Mg^{II}-butylate in the corresponding alcohol under reflux (Linstead's method) and leads (Scheme 1) to the solvated Mg^{II} porphyrazines [TTDPzMg(H_2O)] (**3**) or [TSeDPzMg(H_2O)] (**4**) with 50–70% yield [14,16]. The presence of coordinated water in these two Mg^{II} complexes has been established experimentally, in line with parallel observations for similar tetrapyrrolic systems, including the phthalocyanine Mg^{II} species [35,36]. Demetalation of the Mg^{II} complexes to form the free-base macrocycles **5** and **6** can be best achieved in CF_3COOH. Short treatment with 94–98% H_2SO_4 is applicable for demetalation of the Se-complex [TSeDPzMg(H_2O)] (**4**), but not for the sulfur analogue [TTDPzMg(H_2O)] (**3**), due to rapid hydroprotolytic destruction of the latter (in 96.6% H_2SO_4 $\tau_{1/2} = 21$ and 1.3 min for **6** and **5**, respectively [22]).

Both series of symmetrical metal derivatives [TTDPzM] (**7**) and [TSeDPzM] (**8**) (M = Mn^{II}, Fe^{II}, Co^{II}, Ni^{II}, Cu^{II}, Zn^{II}) could be prepared only by incorporating the metal centers into the free-bases **5** and **6** with MX_2 salts in a coordinating solvent (pyridine, DMSO). Table 1 lists the reactants, products formed, and yields for all the symmetrical S- and Se-porphyrazines so far reported.

The unsuccessful attempts of template macrocyclization reactions starting from the dicyano precursors **1** and **2** and bivalent metal salts, a method applicable to the synthesis of the metal phthalocyanines [PcM], is likely to be due to the known N or S(Se) coordinating ability of 1,2,5-thia- and 1,2,5-selenodiazoles, as shown by the formation of d metal complexes [37–41]. External coordination by thiadiazole rings can also plausibly explain the observed exceeding content of copper in the samples of [TTDPzCu] obtained from dinitrile **1** and copper powder by Moerkved et al. [42]. Noteworthy, template macrocyclization is not an exclusive property of Mg^{II}. In fact, direct cyclotetramerization of dinitrile **1** has just been shown to occur easily with p metal salts [23]. Thus, reaction of **1** in hot quinoline with Al^{III} or Ga^{III} halides leads to the "S-porphyrazines" [TTDPzM(X)] (**9a–c**), whereas the In^{III} complex [TTDPzIn(OAc)] (**9d**) is better obtained by complexation of [TTDPzH$_2$] with In^{III} acetate in acetic acid under reflux (Scheme 1).

Tetrakis(thia/selenodiazole)porphyrazines are very poorly soluble in common organic solvents such as hydrocarbons and their chlorinated derivatives, but they gain higher solubility in donor solvents (pyridine, DMF, DMSO) due to the specific solvation occurring at the central NH groups in the free-base macrocycle or at the coordinatively unsaturated metal centers in its metal derivatives. Some solubility is also achieved in acidic solvents (CF_3COOH, H_2SO_4) due to proton interaction with the *meso*- and heterocyclic N atoms. The presence of peripheral heterocycles also determines also a strong tendency of the solid samples to retain clathrated water and/or carboxylic acids. Indeed, all solid samples are usually obtained as highly solvated materials (see Table 1) and the number of solvent molecules (water, carboxylic acids) can vary from one preparation to another. These molecules can be eliminated upon heating in vacuum, but hydrated samples are normally reformed upon exposition to air. Tetrakis(thiadiazole)porphyrazines, unlike their Se-analogues, can be sublimed in a high vacuum [14,15] or under a slow flow of inert gas [27,28] giving materials or films with different crystallinity.

2.2. Low-symmetry thia/selenodiazoloporphyrazines

Porphyrazines carrying less than four annulated thiadiazole or selenodiazole rings are also known and their structure, spectroscopic and some other physicochemical properties have been studied [20,21,24,25,29–31,43–45]. Scheme 2 shows the full series of symmetrical and low-symmetry thia/selenodiazoloporphyrazines possibly formed by reaction of **1** or **2** in a template co-cyclotetramerization process with

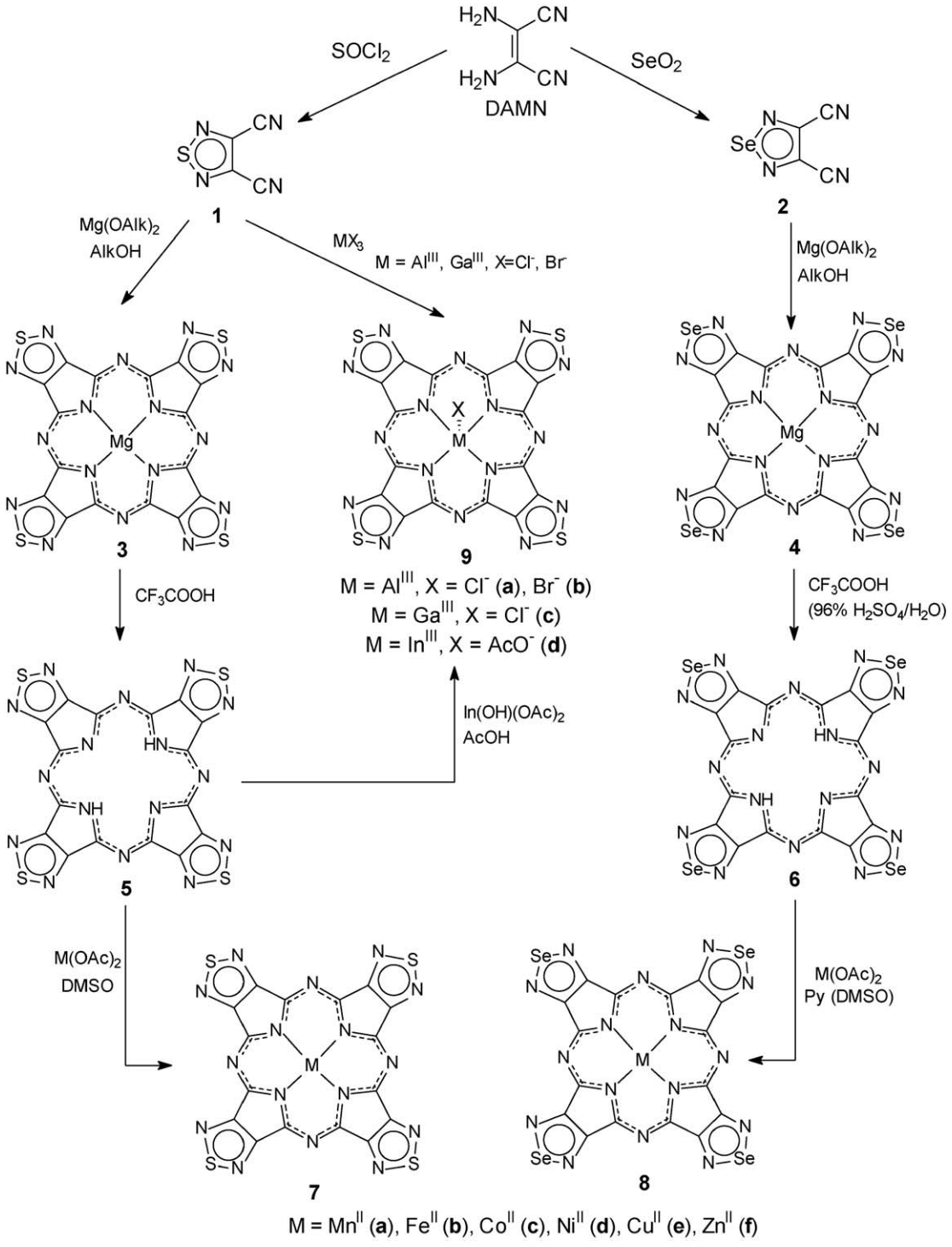

Scheme 1.

different precursors. Chart 3 shows the co-reactants used in the cited reports, namely substituted phthalodinitriles **10** [20,21] and **11** [24], dipropylmaleodinitrile **12** [29] and aryl substituted fumarodinitriles **13** [43,45,46] and **14** [31]. Table 2 lists the series of the corresponding low-symmetry porphyrazines so far effectively isolated and studied.

As shown in Scheme 2, the synthetic approach, in principle quite simple, leads to a mixture of two symmetrical porphyrazines (AAAA and BBBB) and four low-symmetry porphyrazines (AAAB, AABB, ABAB and ABBB). If the two dinitrile precursors, having equal reactivity, are taken in a 1:1 molar ratio, and their co-macrocyclization occurs in a two-step mechanism [47,48] first implying the formation of dimeric units followed by their coupling in the ultimate step, then the amounts of low-symmetry porphyrazines formed should be in the order AABB > AAAB, ABBB > ABAB [24].

Table 1
Synthesis of tetrakis(thiadiazole)- and tetrakis(selenodiazole)porphyrazines [14–17]

M	No.	Synthetic procedures	Solvated form	Yield
Tetrakis(1,2,5-thiadiazole)porphyrazines				
$2H^{I}$	**5**	**3** + CF_3COOH	[TTDPzH_2]	35
Mg^{II}	**3**	Dinitrile **1** + $Mg(OAlk)_2$	[TTDPzMg(H_2O)]·(H_2O)·(AcOH)	47
Mn^{II}	**7a**	**5** + $Mn(OAc)_2$ in DMSO	[TTDPzMn(DMSO)$_2$] → [TTDPzMn]	70
Fe^{II}	**7b**	**5** + $(NH_4)_2Fe(SO_4)_2$ in DMSO	[TTDPzFe(DMSO)$_2$] → [TTDPzFe]	85
Co^{II}	**7c**	**5** + $Co(OAc)_2$ in DMSO	[TTDPzCo]·2(H_2O)	83
Ni^{II}	**7d**	**5** + $Ni(OAc)_2$ in DMSO	[TTDPzNi]·2(H_2O)	70
Cu^{II}	**7e**	**3** + $Cu(OAc)_2$ in CF_3COOH	[TTDPzCu]	44
		5 + $Cu(OAc)_2$ in pyridine	[TTDPzCu]	62
Zn^{II}	**7f**	**5** + $Zn(OAc)_2$ in DMSO	[TTDPzZn]·2(H_2O)	90
Al^{III}	**9a**	Dinitrile **1** + $AlCl_3$ in quinoline	[TTDPzAlCl]·4(H_2O) (quinoline)	56
	9b	Dinitrile **1** + $AlBr_3$ in quinoline	[TTDPzAlBr]·4(H_2O) (quinoline)	39
Ga^{III}	**9c**	Dinitrile **1** + $GaCl_3$ in quinoline	[TTDPzGaCl]·2(H_2O) (quinoline)	35
In^{III}	**9d**	**5** + In(OH)$(OAc)_2$ in AcOH	[TTDPzIn(OAc)]·2(H_2O)	55
Tetrakis(1,2,5-selenodiazole)porphyrazines				
$2H^{I}$	**6**	**4** + CF_3COOH	[TSeDPzH_2]·3(H_2O)·(CF_3COOH)	65
		4 + 96% H_2SO_4/ice	[TSeDPzH_2]·3(H_2O)·(AcOH)	50
Mg^{II}	**4**	Dinitrile **2** + $Mg(OPr)_2$	[TSeDPzMg(H_2O)]·3(H_2O)·(AcOH)	70
Mn^{II}	**8a**	**6** + $Mn(OAc)_2$ in DMSO	[TSeDPzMn]·4(H_2O)·(AcOH)	67
		In pyridine	[TSeDPzMn(py)]·2(H_2O)·(AcOH)	61
Co^{II}	**8c**	**6** + $Co(OAc)_2$ in DMSO	[TSeDPzCo]·5(H_2O)·(AcOH)	69
		In pyridine	[TSeDPzCo(py)]·3(H_2O)·(AcOH)	51
Ni^{II}	**8d**	**6** + $Ni(OAc)_2$ in DMSO	[TSeDPzNi]·6(H_2O)·(AcOH)	72
		In pyridine	[TSeDPzNi(py)]·4(H_2O)·(AcOH)	60
Cu^{II}	**8e**	**4** + $Cu(OAc)_2$ in CF_3COOH	[TSeDPzCu]·3(H_2O)·(AcOH)	47
Zn^{II}	**8f**	**6** + $Zn(OAc)_2$ in DMSO	[TSeDPzZn]·4(H_2O)·(AcOH)	61
		In pyridine	[TSeDPzZn]·5(H_2O)·(AcOH)	48

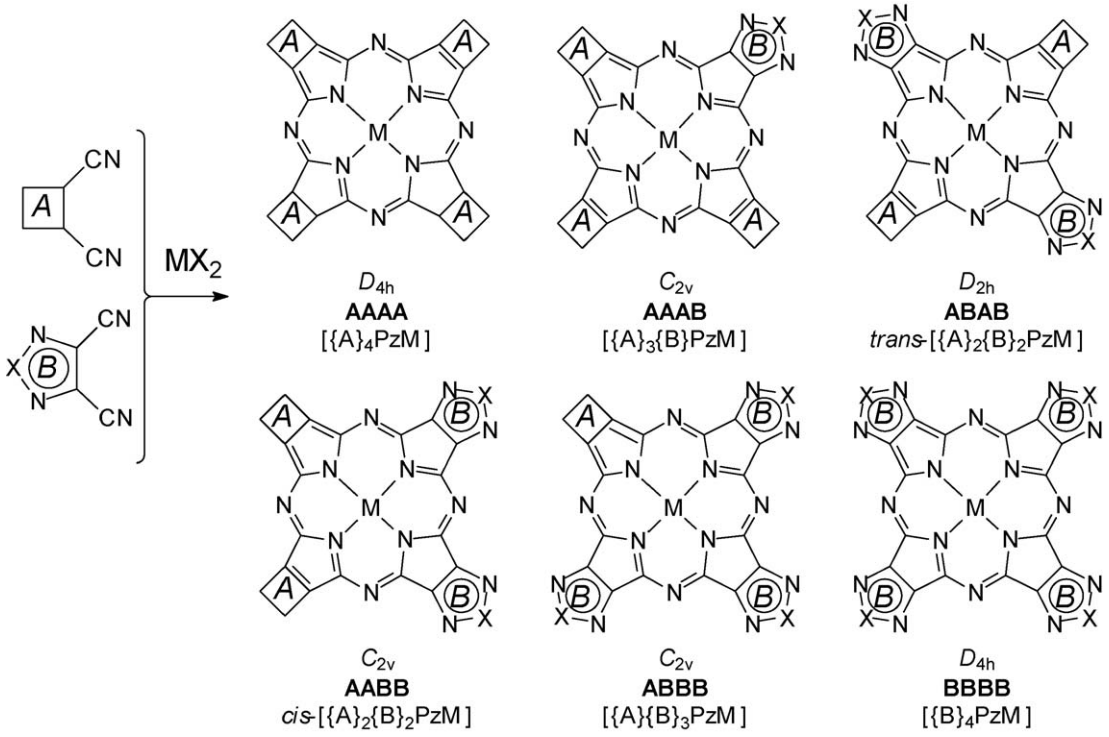

Scheme 2.

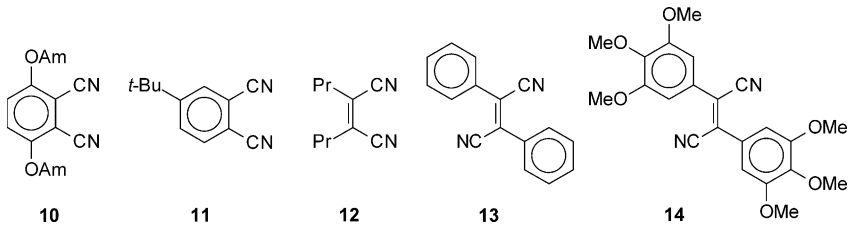

10 11 12 13 14

Chart 3.

Table 2
Low-symmetry thia/selenodiazoloporphyrazines

A	B	Substitution pattern	No.	Abbreviation	M	Ref.
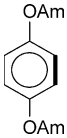	X = S	**AAAB**	**15**	[SA_3PzM]	2H (**a**), Mg (**b**)	[20,21]
		ABAB	**16**	[SASAPzM]	2H (**a**), Mg (**b**)	[21]
		AABB	**17**	[S_2A_2PzM]	2H (**a**), Mg (**b**)	[21]
		ABBB	**18**	[S_3APzM]	2H (**a**), Mg (**b**)	[21]
	X = Se	**AAAB**	**20**	[SeA_3PzM]	2H (**a**)	[20]
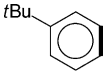	X = S	**AAAB**	**21**	[SB_3PzM]	2H (**a**), Mg (**b**), Cu (**c**)	[24]
		AABB	**22**	[S_2B_2PzM]	Mg (**b**)	[24]
[Ph]$_2$	X = S	**AAAB**	**23**	[Ph_6SPzM]	2H (**a**), Zn (**b**)	[43,46]
	X = Se	**AAAB**	**24**	[Ph_6SePzM]	2H (**a**), Mg (**b**), Cu (**c**), Zn (**d**)	[45,46]
[3,4,5-(MeO)$_3$Ph]$_2$	X = Se	**AAAB**	**25**	–	2H (**a**), Mg (**b**), Cu (**c**)	[31]
[Pr]$_2$	X = Se	**AAAB**	**26**	[Pr_6SePzM]	2H (**a**), Mg (**b**), Ni (**c**), Cu (**d**), ClMn (**e**)	[29–31]

According to semiempirical calculations (AM1 and PM3 methods), the C≡N bonds in **1** and **2** are more strongly polarized than in phthalodinitriles [21] and maleodinitriles and, unlike the two latter species, the cyano groups in **1** and **2** have a positively charged N atom (Table 3). As a consequence, a relatively higher reactivity is expected for **1** and **2** in cyclocondensation reactions.

The main drawback of the co-macrocyclization approach (Scheme 2) consists of the very elaborated chromatographic procedures required for the isolation of each single pure porphyrazine macrocycle present in the mixture. The yield of the goal low-symmetry porphyrazine can be optimized to some extent by appropriately modifying the ratio of the reacting dinitriles *A* and *B* and by the reaction conditions of the template condensation.

Table 3
Atomic charges on the cyano groups in some dinitriles obtained by PM3 method

Dinitrile	Atomic charges		Polarization of CN bond, $\Delta\delta$
	$\delta_{C\equiv}$	$\delta_{\equiv N}$	
1,2,5-Thiadiazolo-3,4-dicarbonitrile (**1**)	−0.108	+0.022	0.130
1,2,5-Selenodiazolo-3,4-dicarbonitrile (**2**)	−0.116	+0.024	0.140
Phthalodinitrile	−0.114	−0.028	0.086
tert-Butylphthalodinitrile (**11**)	−0.110	−0.032	0.078
3,6-Diamyloxyphthalodinitrile (**10**)	−0.098	−0.032	0.066
Maleodinitrile	−0.137	−0.018	0.119
Dipropylmaleodinitrile (**12**)	−0.116	−0.031	0.085
Diphenylmaleodinitrile *cis*-(**13**)	−0.125	−0.024	0.101

The full series of low-symmetry thiadiazolobenzoporphyrazines **15–18** (Table 2) were obtained by us from the template condensation of dinitrile **1** and the amyloxysubstituted phthalodinitrile **10** [20,21] in boiling *n*-amyl alcohol in the presence of lithium or magnesium amylates. The reaction conditions were deeply studied. When lithium amylate was used as a template agent and the reaction mixture was then acidified by acetic acid, the two symmetrical porphyrazines [$(AmO)_8PcH_2$] (AAAA (**19**)) and [$TTDzPzH_2$] (BBBB (**5**)) were obtained in mixture with the four low-symmetry porphyrazines **15a–18a** (AAAB, ABAB, AABB, ABBB) and, after tedious chromatographic procedures, **15a** (AAAB), **16a** (ABAB) and **17a** (AABB), were isolated as pure species. The relative yield of **15a** (AAAB) could be increased when the reaction was conducted with an excess of dinitrile **10** with respect to **1**. Although the use of magnesium amylate as a template agent requires an additional step, i.e. demetalation of the mixture of the Mg^{II} complexes by treatment with trifluoroacetic acid, this procedure showed some advantages. First, no symmetrical octaamyloxyphthalocyanine, [$(AmO)_8PcH_2$] (AAAA), was formed in this case; secondly, when dinitrile **10** was pre-heated for 10–15 min before addition of the dinitrile **1** the yield of the *cis*-porphyrazine **17a** (AABB) was increased. In addition, the porphyrazine **18a** with three thiadiazole rings (ABBB) could be chromatographically separated only as Mg^{II} complex and only then converted into the free-base, since this latter cannot be eluted even with pyridine. In all cases, considerable amounts of the symmetrical species **5**, [$TTDPzH_2$], were formed, in line with the higher activity expected for the heterocyclic dinitrile **1**. Low-symmetry porphyrazines **15a** (AAAB) and **17a** (AABB)

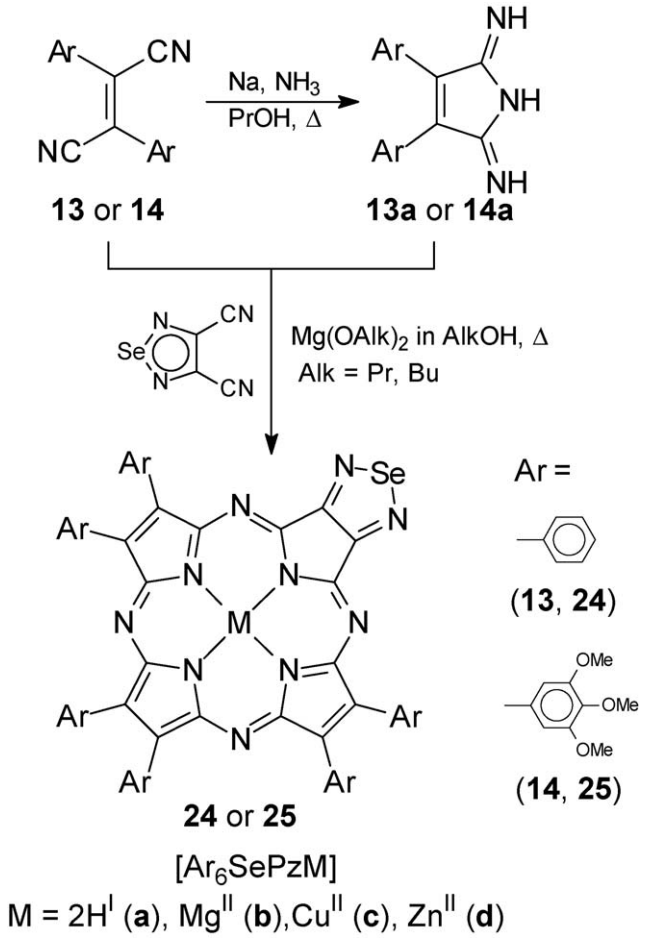

Scheme 3.

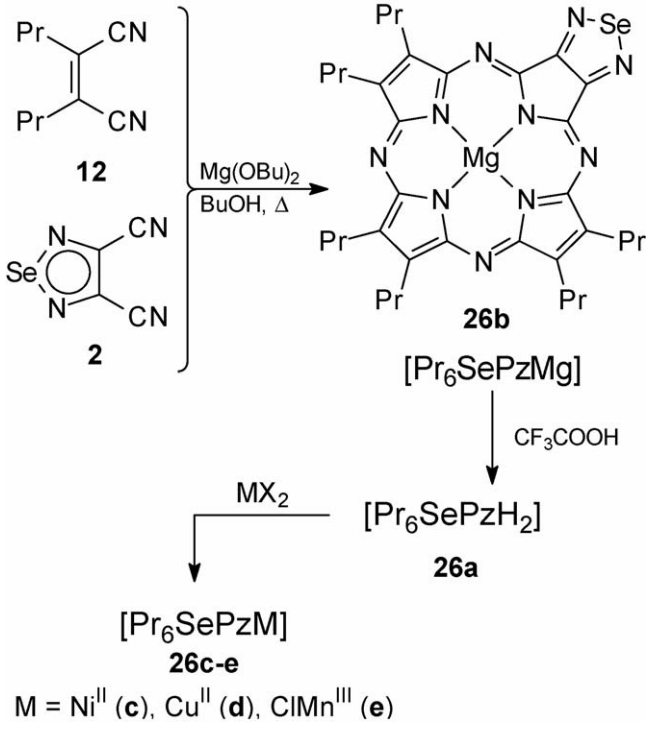

Scheme 4.

were obtained as single crystals and their structure has been elucidated by X-rays [20,21]. Moreover, co-condensation of the Se-containing dinitrile **2** and the phthalodinitrile **10** in the presence of magnesium amylate led to isolation of the Se-porphyrazine **20a** (Scheme 2, Table 2) [20], which was found by single-crystal X-ray work to be isostructural with S-porphyrazine **15a**.

Template condensation of dinitrile **1** with *tert*-butylphthalodinitrile **11** (1:1.2 molar ratio) in the presence of magnesium butylate in *n*-butanol led to a mixture of Mg^{II}-porphyrazines from which fractions containing low-symmetry Mg^{II}-porphyrazines **21b** and **22b** were isolated. These two species were characterized on the basis of elemental analysis, mass- and UV–vis spectra [24]. Treatment of **21b** with CF_3COOH afforded the free-base **21a**.

By co-condensation of the dinitriles **1** or **2** with diphenylfumarodinitrile **13** in the presence of $Mg(OBu)_2$ in *n*-butanol (Scheme 3), β-phenyl substituted porphyrazines **23** and **24**, bearing one thia- or selenodiazole unit, were also prepared (Table 2; $M = 2H^I$, Zn^{II}) [45,46]. Demetalation of the initially formed mixture of Mg^{II} complexes facilitated the chromatographic separation of the individual low-symmetry free-bases **23a** and **24a**, which were then converted, by treatment with the appropriate metal acetates in pyridine, to the corresponding Zn^{II} complex **23d** and Cu^{II} and Zn^{II} complexes **24c** and **24d**, respectively. Since the dinitriles **13** and **14** have a *trans* configuration, their *trans* → *cis* isomerization is required prior to the effective co-cyclocondensation to afford the low-symmetry porphyrazine macrocycle. Such isomerization can be facilitated if the *trans*-dinitrile is preliminarly treated with NH_3 in an appropriate alcohol (methanol, propanol or butanol) in the presence of sodium alcoholate – a process which leads to the diiminoimide intermediate **13a** (**14a**) (Scheme 3) – a reactive species in the cyclocondensation reaction. This approach was used [31] in the case of 3,4,5-trimethoxysubstituted diphenylfumarodinitrile **14**, which was converted to diiminoimide **14a** and this latter was then co-condensed with the Se-containing dinitrile **2** in the presence of $Mg(OPr)_2$ in propanol to give the Mg^{II} porphyrazine **25b** in a 14% yield. This species after demetallation with CF_3COOH to **25a** was converted to the Cu^{II} complex **25c**. These 3,4,5-trimethoxylated hexaphenylporphyrazines show enhanced solubility in organic solvents.

The Se-dinitrile **2** was also used by the Barrett–Hoffman group [29] in a co-cyclization reaction with seven-fold excess of dipropylmaleodinitrile **12** in the presence of Mg^{II} butylate in *n*-butanol and the Mg^{II} complex of hexapropyl(selenodiazole) porphyrazine, [$Pr_6SePzMg$] **26b** was obtained in 42% yield (Scheme 4). The structure of the mono-aquo-complex [$Pr_6SePzMg(H_2O)$] has been solved by an X-ray diffraction study [29] (see below Fig. 9). Demetalation of the Mg^{II} complex with CF_3COOH afforded the corresponding free-base [Pr_6SePzH_2] **26a** in 70% yield, which was then metalated with Cu^{II} and Ni^{II} salts to give the corresponding complexes **26c** and **26d** [31]. The reaction of [Pr_6SePzH_2] with $MnCl_2$ in the pres-

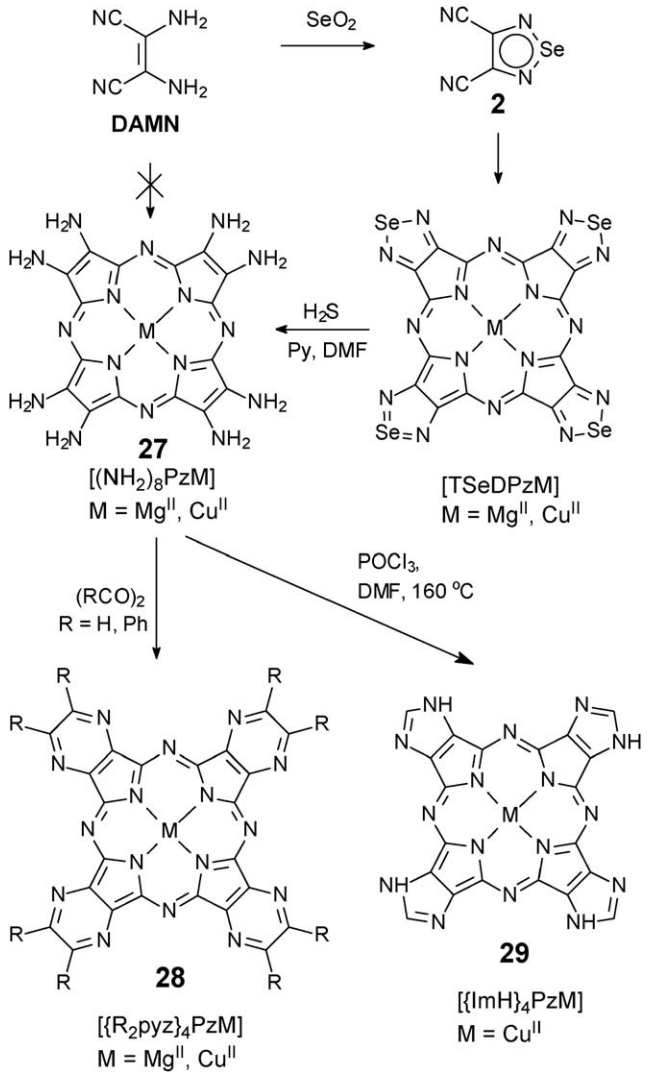

Scheme 5.

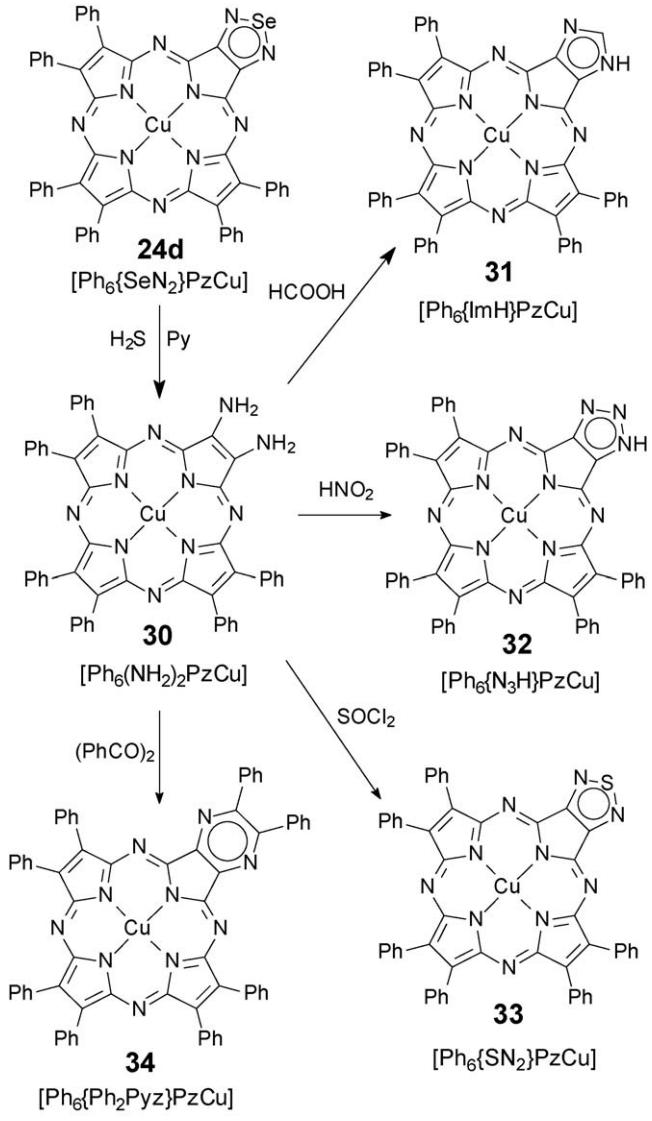

Scheme 6.

ence of O_2 leads to formation of Mn^{III} complex [Pr_6SePzMnCl] **26e** (Scheme 4) [30].

2.3. Deselenation of Se-porphyrazines—a route to vicinal diamino functionalities and to octaaminoporphyrazine

One of the most relevant forms of reactivity shown by the Se-porphyrazines is that the annulated selenodiazole rings can undergo reductive ring opening under the action of H_2S with releasing of the Se atom and formation of vicinal diamino functionalities which are open to possible different kinds of derivatization, as will be shown below. Attempts to directly form porphyrazines carrying vicinal NH_2 groups from diaminomaleodinitrile (Scheme 5) were unsuccessful [12]. It was first recognized by us in 1999 [16] that the deselenation process could be applied to the symmetrical Mg^{II} and Cu^{II} complexes [TSeDPzMg] (**4**) and [TSeDPzCu] (**8e**) by bubbling H_2S into a pyridine (or DMF) solution. The process leads (Scheme 5) to the formation of the corresponding octaaminoporphyrazines [$(H_2N)_8$PzM] (**27**) which cannot be isolated as pure solid materials due to their instability. Nevertheless, once prepared, they can be straightforwardly used in situ for further transformations, as is exemplified in Scheme 5 for their conversion to pyrazinoporphyrazines [$(R_2Pyz)_4$PzM] (**28**) by reaction with α-dialdehydes [16], or to an imidazole derivative [$(ImH)_4$PzM] (**29**) by reaction with DMF in the presence of $POCl_3$ [12].

The selenodiazole rings in low-symmetry porphyrazines can be also cleaved and deselenated under similar experimental conditions. Release of selenium from mono(selenodiazole) porphyrazines affords the corresponding porphyrazines carrying one external vicinal diamino functionality first obtained for tribenzoporphyrazine **20a** and hexaphenylporphyrazine **24d** [45]. By reaction of **30** obtained in situ with different electrophiles (Scheme 6), ring reclosure takes place and imidazo-, 1,2,3-triazolo-, 1,2,5-thiadiazolo- and pyrazinoporphyrazines, **31**–**34**, are formed [12,45].

The deselenation process was also applied [29] for the conversion of hexapropyl substituted monoselenodiazoleporphyrazine **26** to the corresponding vicinal diaminoderivative

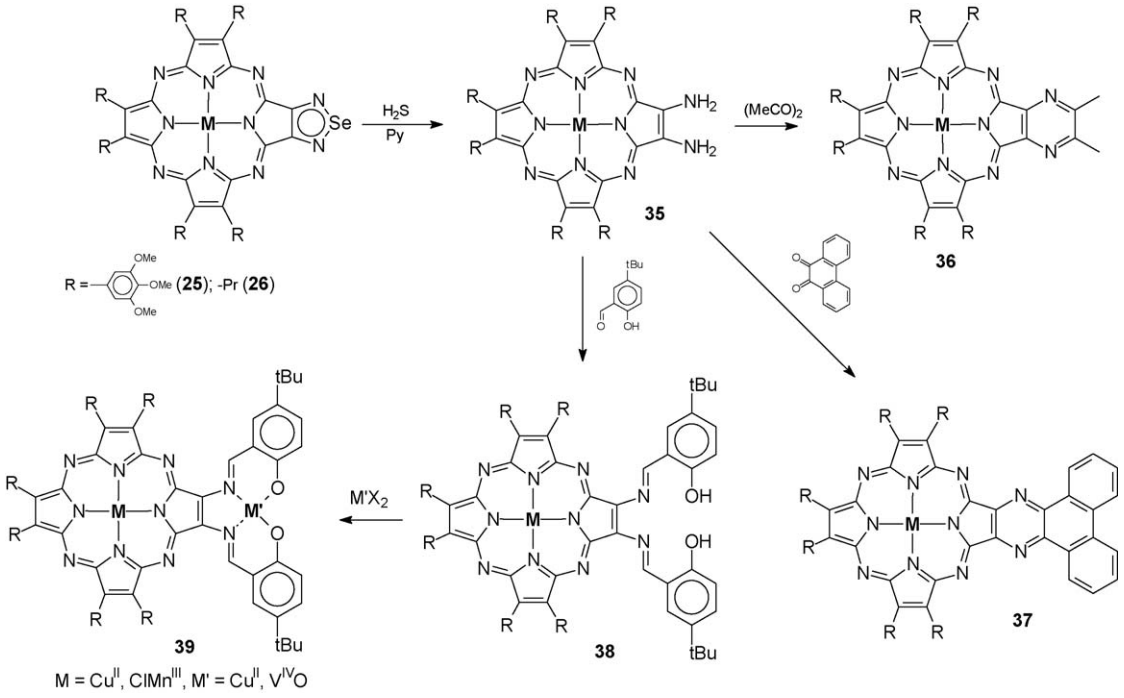

Scheme 7.

35, this latter directly converted in situ with 2,3-butanedione or 9,10-phenanthrenedione affording the corresponding substituted tetrapyrazinoporphyrazines **36** and **37** (Scheme 7). The same authors have used deselenation of β-trimethoxyphenyl and β-propyl substituted mono(selenodiazole)porphyrazines **25** and **26** for the preparation of the Schiff-base adducts of the vicinal diaminoporphyrazines **38** (Scheme 7). These latter were then converted to the dinuclear porphyrazinato-Schiff-base complexes **39** which can be considered as molecular scaffolds for the design of strongly spin-coupled "ferrimagnetic" systems with high residual spin [30,31,44].

3. Crystal and molecular structure

Very recent single-crystal X-ray studies have considerably expanded the amount of structural information on a series of low-symmetry and symmetrical "S- and "Se-porphyrazines". Elucidated structures were those of the low-symmetry free-bases **15a** and **17a** (Table 2) containing one [20,21] and two [21] annulated thiadiazole rings, respectively, and of the symmetrical unmetalated species **5**, [$TTDPzH_2$] [27]. In the context of the work carried out on the symmetrical and low-symmetry series formed by annulation externally to the porphyrazine core of diamyloxybenzene and thiadiazole rings the structure of the symmetrical octaamyloxyphthalocyanine [$(AmO)_8PcH_2$] **19** has also been elucidated [21]. Thus, four out of six macrocycles of the series **5**, **15a**–**18a**, **19**, schematically shown in Scheme 2, have known structures clarified by X-ray work. To our knowledge, this fact is unprecedented in the field of tetrapyrrolic macrocycles. Structures of two porphyrazines with one annulated selenodiazole ring – free-base **20a** [20] and the Mg^{II} complex **26b** [29] – have also been investigated. These studies have not only established the influence of heterocyclic annulation on the geometrical structure within each individual macrocycle, but they also revealed its remarkable effect on the ability of macrocycles to generate intermolecular interactions determining the observed peculiar and characteristic molecular packing in the crystals (see here below).

The X-work for the symmetrical "S-porphyrazines" has been extended to include the series of the metal derivatives of the free-base **5**, [$TTDPzH_2$], with divalent 3d transition metals, TTDPzM (**7a–7e**, M = Fe^{II}, Co^{II}, Ni^{II}, Cu^{II}, Zn^{II}) [27,28]. This extensive work is so rich in achieved structural information (see below) to be a milestone in the field of tetrapyrrolic macrocycles, certainly at least comparable with the overall X-ray crystallographic work which has been developed along several decades for the parallel series of phthalocyanine macrocycles [PcM] (M = $2H^1$, Fe^{II}, Co^{II}, Ni^{II}, Cu^{II}, Zn^{II}) since the pioneering Robertson's work in the 1930s [49]. On the "S-porphyrazines" further X-ray work has just been reported for the metal derivatives of the TTDPz macrocycle with tervalent p metals, i.e. [TTDPzMCl] (M = Al^{III} and Ga^{III}) **9a** and **9c** [23].

3.1. Solid state arrangement

With reference to the series of symmetrical and low-symmetry macrocycles shown in Scheme 2, it is illustrative to consider how gradual substitution of benzene moieties in amyloxysubstituted phthalocyanine [$(AmO)_8PcH_2$] by thiadiazole rings changes the molecular packing pattern in the crystals. Fig. 1(top) shows that in the molecules of [$(AmO)_8PcH_2$] [21] some waving distortion from planarity occurs due to steric interaction of adjacent amyloxy chains. Also, the mean planes of the molecules are parallel to one another, but neighbouring

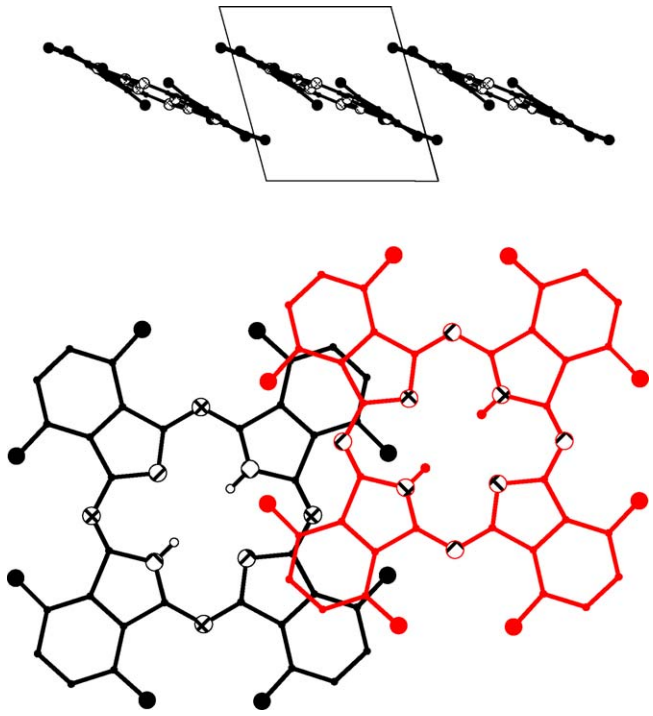

Fig. 1. Crystal packing of [$(AmO)_8PcH_2$] (**19**): view along the *c*-axis (top) and perpendicularly to the mean plane of the macrocycle (bottom). Alkyl chains are not shown. Figure produced using data from Ref. [21].

molecules overlap only by edges of their conjugated π systems (Fig. 1, bottom). The closest intermolecular contacts are ca. 3.5–3.6 Å (e.g. the shortest C_α(pyrrole)···C_β(benzene) is 3.501 Å) and any significant intermolecular π–π interaction can be excluded.

Substitution of one of the benzene moieties by a thiadiazole ring as in **15a** (AAAB) [20,21] leads to a strong polarization of the macrocyclic π system ("push–pull" effect) with implied intermolecular dipole–dipole interactions. These effects determine the observed arrangement of the macrocycles in centrosymmetric pairs (Fig. 2, top) this resulting in short intemolecular contacts (ca. 3.3 Å, $C_\alpha\cdots C_\alpha$ is 3.298 Å). A similar form of intermolecular arrangement and short contacts are observed in the isomorphous crystal structure of **20a** [20] in which a single annulated selenodiazole ring substitutes the thiadiazole ring present in **15a**. Short intermolecular distances associated with considerable overlap of the macrocyclic π systems in the centrosymmetric pair (Fig. 2, bottom) are plausibly responsible for the presence of a strong π–π interaction. It is interesting that overlapping macrocycles are slipped along the $N_{pyr}\cdots N_{pyr}$ axis, a feature shared by the x-polymorphs of phthalocyanine, x1-[PcH_2] and x2-[PcH_2] [50–52], but the degree of overlap is higher in the structures **15a** and **20a**. This type of molecular overlap is different from that present in the well known α- and β-forms of [PcH_2] which are slipped along $N_{meso}\cdots N_{meso}$ axes [52]. Hydrogen bonding interactions of amyloxy chains with thia/selenodiazole rings and *meso*-N atoms contribute to the bonding within the dimeric units of **15a** and **20a**. Despite the lower steric hindrance between amyloxy groups in **15a** as compared to [$(AmO)_8PcH_2$], the distortion from planarity of

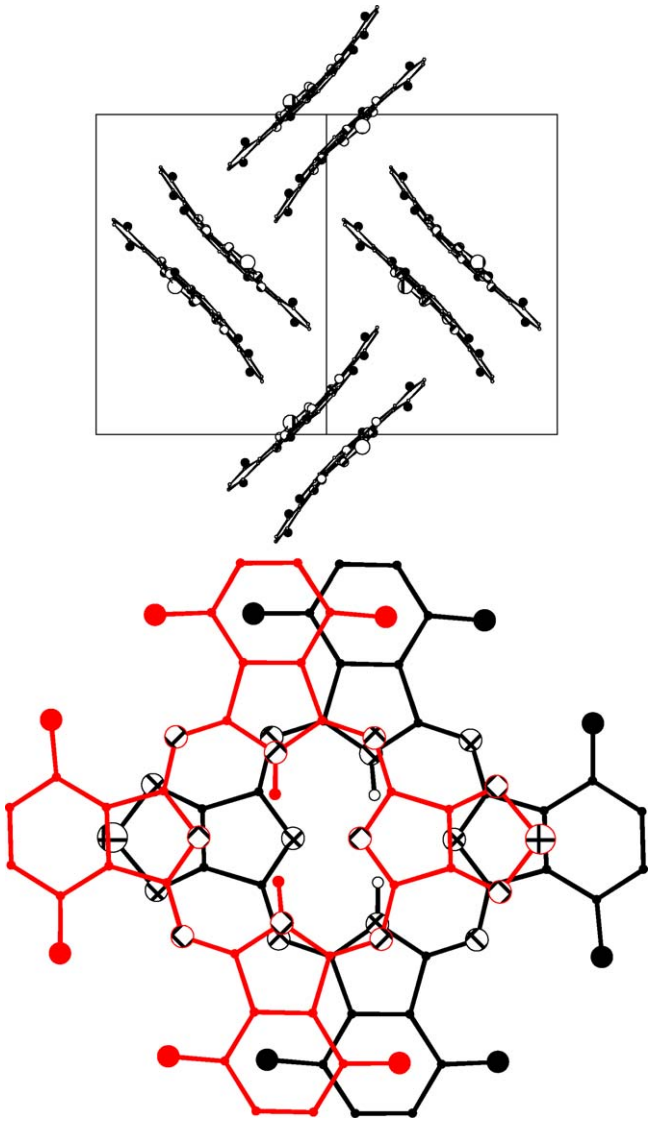

Fig. 2. Crystal packing of **15a**: view along the (1 0 1) axis (top) and perpendicular to the mean plane of the macrocycle (bottom). Alkyl chains are not shown. Figure produced using data from Refs. [20,21].

the macrocycle containing one thia/selediazole ring is increased resulting from dipole–dipole interaction.

Annulation of two thiadiazole rings to pyrrole rings in relative adjacent position as in the porphyrazine macrocycle **17a** (AABB) [21] also induces polarization of the macrocyclic π system ("push–pull" effect) and formation of molecular pairs (Fig. 3A). In **17a**, the interunit contacts reach values as short as 3.2–3.3 Å ($C_\alpha\cdots C_{meso}$ 3.249 and C_α(pyrrole)···C_β(benzene) 3.248 Å, $N_{pyr}\cdots N_{pyr}$ 3.335 Å). The slipping of the molecules in the pair along the $N_{pyr}\cdots N_{pyr}$ axis (Fig. 3B) is larger than in the case of the monothiadiazole annulated species **15a**, which plausibly weakens the degree of overlap of the π systems. The molecular pairs in **17a** are not isolated as in **15a** but stacked in such way that neighbouring molecules of the adjacent molecular pairs, slipped along the $N_{meso}\cdots N_{meso}$ axis, have the closest interatomic contacts of ca. 3.4 Å ($C_\alpha\cdots N_{pyr}H$ 3.384 Å, $N_{pyr}\cdots C_\alpha$ 3.401 Å, $C_\alpha\cdots C_\alpha$ 3.415 Å and $N_{pyr}\cdots N_{pyr}H$ 3.450 Å). This

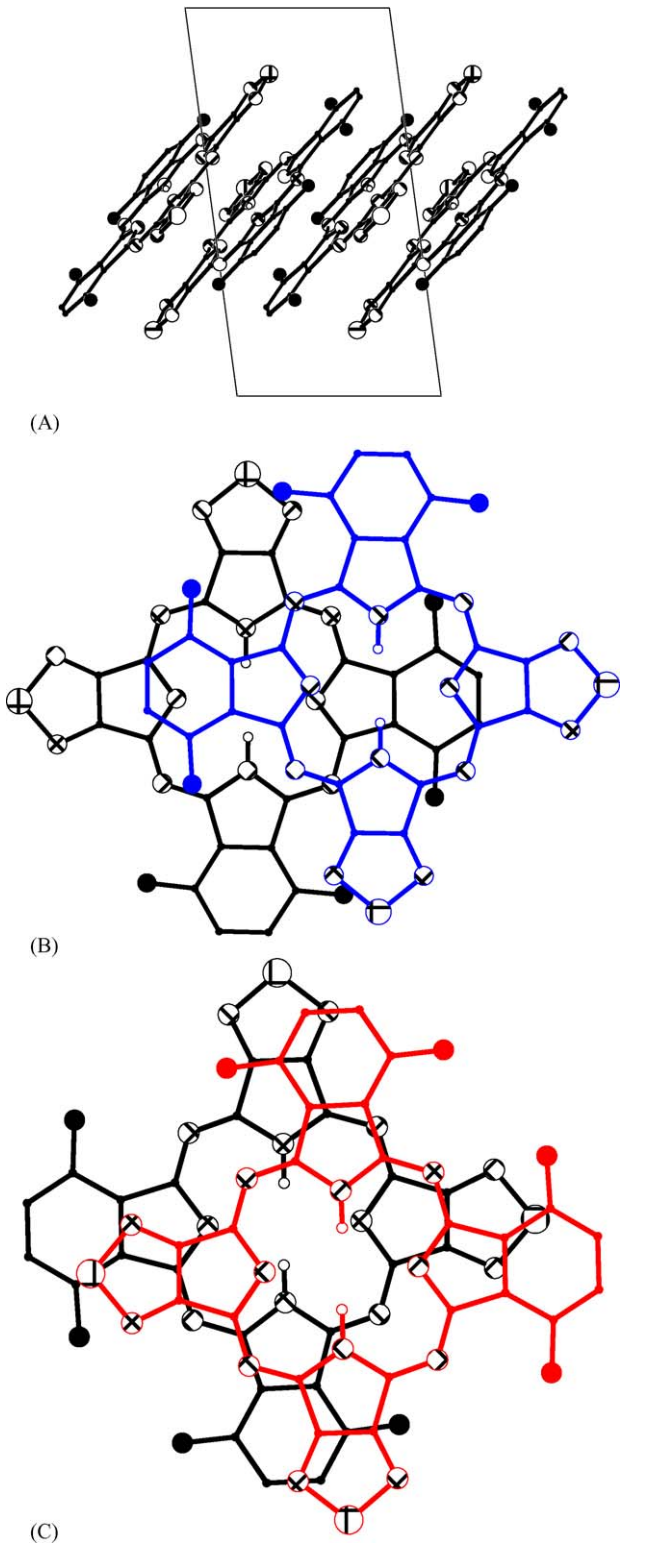

Fig. 3. Stacking of the dimeric units formed by **17a**: (A) view along the *c*-axis, (B) overlap of the molecules in the dimeric unit, and (C) overlap of neighbouring molecules of two adjacent dimers. Alkyl chains are not shown. Figure produced using data from Ref. [21].

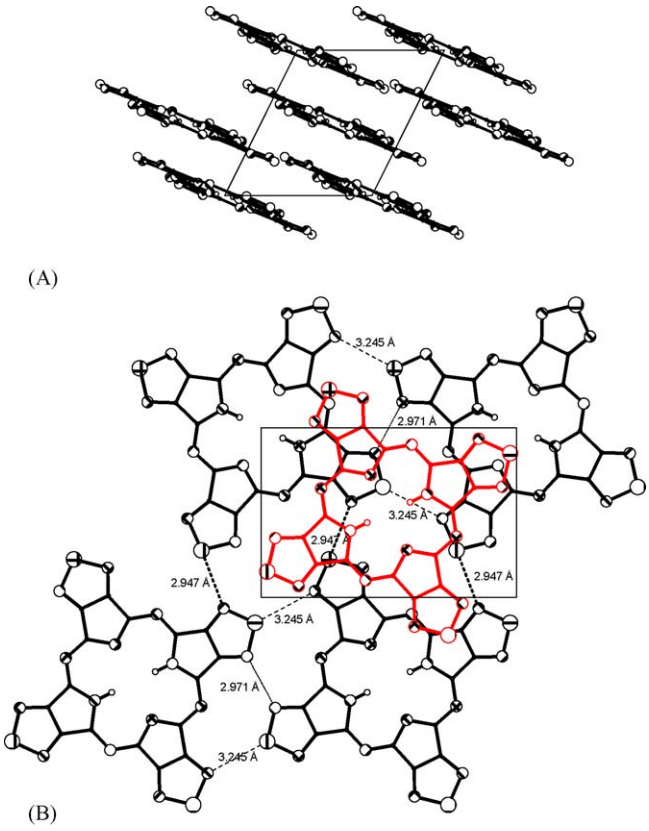

Fig. 4. Molecular packing of α-[TTDPzH$_2$]. Views along the *b*-axis (A) illustrating the layered structure and along the *c*-axis (B) showing the intermolecular contacts within a layer and molecular overlap. Figure produced using data from Ref. [27].

type of stacking only weakly affects the quasi-planar structure of the porphyrazine macrocycle. The overlap with slipping along $N_{meso}\cdots N_{meso}$ axis is characteristic for the β-polymorph of [PcH$_2$], but the degree of overlap is larger in the case of our *cis*-annulated porphyrazine **17a**. Moreover, this species, combining the features of x- and β-polymorphs of phthalocyanine with even stronger π–π overlapping, forms an unprecedented stacked array which might facilitate interunit π-electron transfer.

Let us now consider the effect of the presence of four thiadiazole groups annulated to the central porphyrazine core on the structural arrangement, starting first with the free-base **5**, indicated as α-[TTDPzH$_2$] [27]. The molecular packing (Fig. 4A) has no analogy with that found in any of the polymorphs of the phthalocyanine analogue [PcH$_2$]. In fact, no columnar stacking of the molecules with columns arranged in a parallel fashion is observed. Rather, in α-[TTDPzH$_2$] we might speak of a "graphite-like" structure in which the molecules form parallel infinite layers, intermolecular contacts within each layer occurring between peripheral heteroatoms. The N···S contacts (thick dashed lines in Fig. 4B) are seen with a distance significantly shorter (2.947 Å) than the sum of the S and N van der Waals radii (1.55 + 1.80 = 3.35 Å [53]) and their relative orientation suggests the occurrence of some kind of π–π interaction due to p_z(N)–dπ(S) overlap. Other short intermolecular contacts, shown in Fig. 4B as thin dashed and dotted lines – N···S

Table 4
Different polymorphs formed by [TTDPzH$_2$] and its metal complexes

Compound	Polymorph
[TTDPzH$_2$]	α
[TTDPzCu]	α′, γ
[TTDPzNi]	α, γ
[TTDPzCo]	β
[TTDPzFe]	β
[TTDPzZn]	β
[TTDPzAl(Cl)]	α_2
[TTDPzGa(Cl)]	α_2

(3.245 Å) and N···N (2.971 Å) – are only slightly shorter than the respective van der Waals radii sum (3.35 and 3.10 Å) and hence are probably of less relevant role in regulating intermolecular contacts. As can also be seen from Fig. 4B, each molecule in the bottom layer is overlapped by three molecules of the adjacent top layer; so, there is no consistent overlap of the bottom macrocycle with anyone of the top units. Despite of that, adjacent layers show interlayer contacts as short as 3.2–3.3 Å (e.g. $N_{meso}\cdots C_\alpha$ 3.177 Å, $N_{meso}\cdots C_\beta$ 3.201 Å). This interplane interaction leads to some out-of-plane deformation of the macrocycle, which otherwise should be completely planar. The observed layered structure and short interlayer contacts found for **5** have no counterpart in the case of phthalocyanines.

Some of the features found in the crystal structure of the free-base macrocycle α-[TTDPzH$_2$] are also observed in the structures of its metal derivatives [TTDPzM] (M = Fe^{II}, Co^{II}, Ni^{II}, Cu^{II}, Zn^{II}) [27,28] and [TTDPzMCl] (M = Al^{III}, Ga^{III}) [23]. However, new specific features are introduced which are determined by the oxidation, spin state and coordination properties of each individual metal center. The different polymorphs for [TTDPzH$_2$] and the series of the [TTDPzM] and [TTDPzMCl] species are listed in Table 4.

The Ni^{II} and Cu^{II} complexes form α-polymorphs [28]. The structures, which are denoted as α-[TTDPzNi] and α′-[TTDPzCu], respectively, both consist of parallel two-dimensional layers, arranged in a way similar to what has been found for α-[TTDPzH$_2$] [27]. Each layer is assembled by N···S interactions among thiadiazole rings, but the overlap of the molecules in the adjacent parallel layers is different. α-[TTDPzNi] is practically isomorphous with α-[TTDPzH$_2$] and is formed of identical layers which are shifted along the *a*-axis. The macrocycles have the closest interlayer interatomic contacts of ca. 3.2 Å ($N_{meso}\cdots C_\alpha$ 3.199 Å). The Ni atoms have the closest interplane contact with S atoms, but the Ni···S distance of 3.776 Å excludes any effective coordination interaction between the layers.

In the case of α′-[TTDPzCu], there are five crystallographically independent macrocycles Cu1–Cu5, which are assembled in three different parallel layers, one containing only the Cu1 type of macrocycles, the other two Cu2–Cu3 and Cu4–Cu5 couples (Fig. 5). In each layer, the macrocycles are held together by similar N···S contacts characteristic of the α-polymorph. As seen in Fig. 5A, along the *c*-axis the Cu1 and Cu4–Cu5 layers are each one sandwiched between Cu2–Cu3

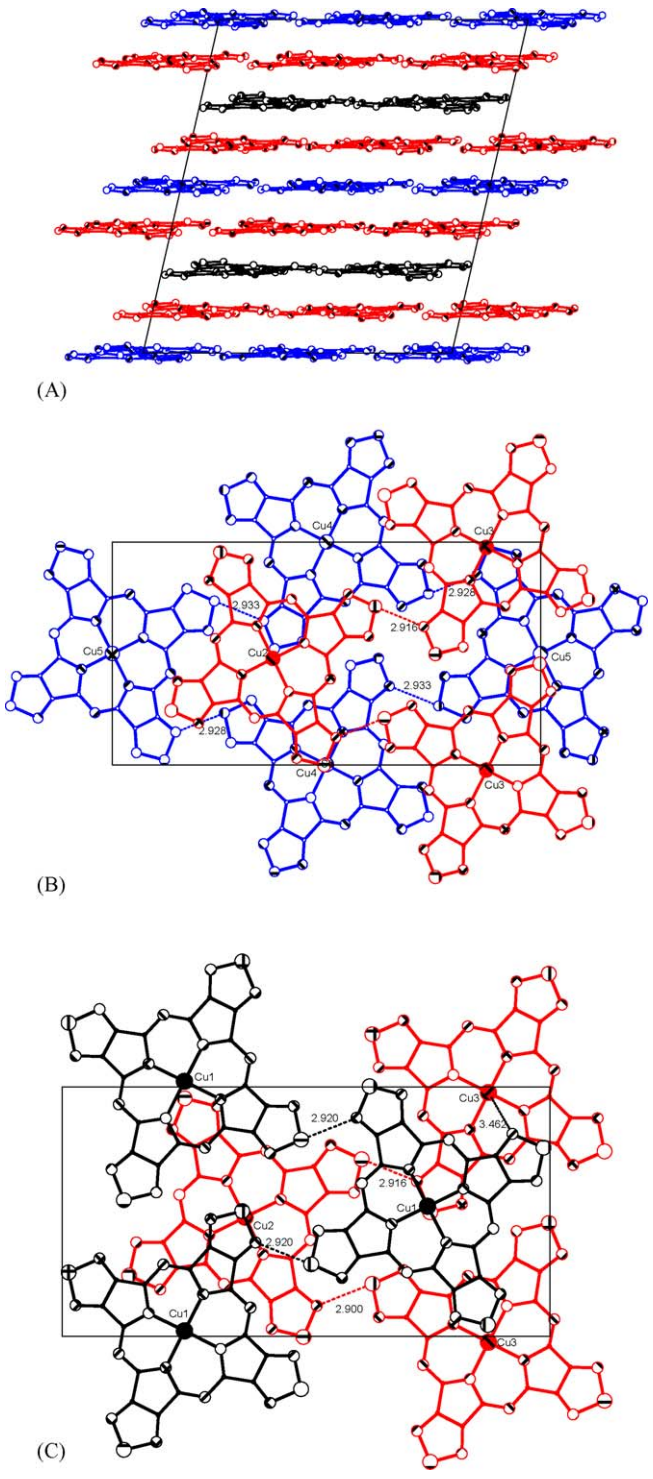

Fig. 5. Layered crystal structure in α′-[TTDPzCu]. (A) View along the *b*-axis. Different layers have different colors: Cu1, black; Cu2 and Cu3, red; Cu4 and Cu5, blue. (B and C) View along the *c*-axis—intermolecular short contacts and overlap of different layers. Figure produced using data from Ref. [28].

layers in the sequence (bottom → top) Cu4–Cu5 → Cu2–Cu3 → Cu1 → Cu2–Cu3 → Cu4–Cu5 → Cu2–Cu3 → Cu1 → Cu2–Cu3 → Cu4–Cu5, etc. Although the average interplane distances (ca. 3.3 Å) approach those found for α-[TTDPzNi] and α-[TTDPzH$_2$], the shortest interplane contacts between the atoms of the macrocycles are in the range 3.1–3.3 Å (e.g.

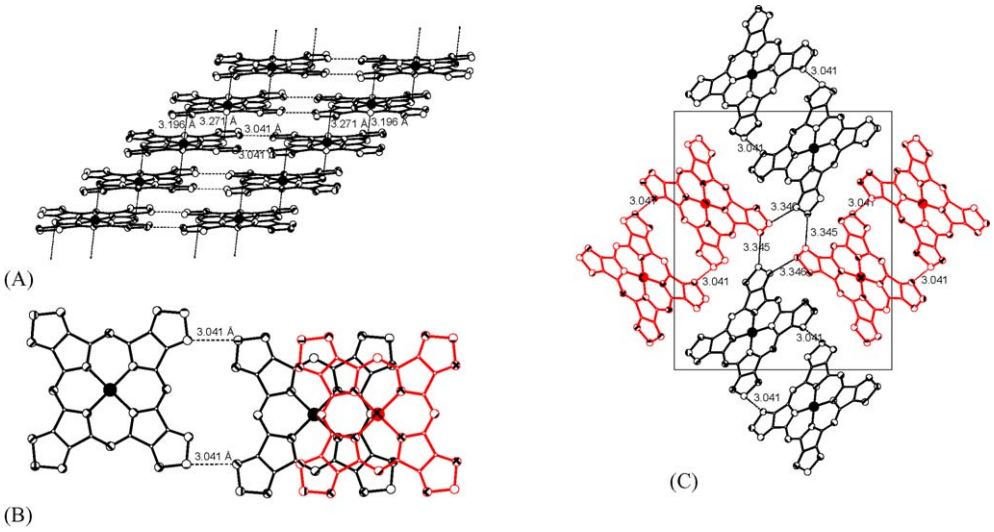

Fig. 6. Molecular packing of γ-[TTDPzCu]: (A) two leg ladder structure, (B) molecular overlap in the ladder, (C) view along the *a*-axis. Short N···S contacts are indicated by dashed lines, the corresponding distances are given in Å. Figure produced using data from Ref. [28].

$N_{meso}\cdots C_{\alpha}$ 3.083 Å, $N_{meso}\cdots$N(thiadiazole) 3.258 Å) and those of Cu^{II} with N and S atoms of the thiadiazole rings (Cu1···N 3.462 Å, Cu···S ca. 3.6 Å) can be indicative of some interlayer π–π interaction somewhat contributed by Cu···N and Cu···S interplane coordination.

As shown in Table 4, the Cu^{II} and Ni^{II} complexes form also γ-polymorphs, i.e. γ-[TTDPzCu] and γ-[TTDPzNi] isomorphous with each other. This γ-polymorph (see Fig. 6 for the Cu^{II} complex) has a characteristic two leg ladder structure forming two parallel columnarly stacked sequences of macrocycles. The edge-to-edge dimers formed by N···S interaction of the thiadiazole rings (3.041 and 3.013 Å for Cu^{II} and Ni^{II} complexes, respectively) are arranged in a staircase-like structure running along the *a*-axis (Fig. 6A). Within the dimeric unit (Fig. 6B), the two macrocycles are slipped along the $N_{meso}\cdots N_{meso}$ axis in such a way that each one of the two Cu^{II} (or Ni^{II}) atoms finds a *meso*-N atom of the neighbouring molecule closely in correspondence of its axial position. Such situation leads to quite short interplane interatomic distances of ca. 3.2 Å (e.g. $Cu\cdots N_{meso}$ 3.196 and 3.271 Å, and $Ni\cdots N_{meso}$ 3.177 and 3.298 Å) and is favourable for considerable interplane π–π overlap. Short N···S contacts (ca. 3.3 Å) are also observed between the molecules in the neighbouring ladders, in which the dimeric units are relatively rotated by ca. 60° (Fig. 6C).

The TTDPz complexes with Fe^{II}, Co^{II} and Zn^{II}, metal ions more suitable for axial ligation, form a unique β-polymorph [27,28]. It is extremely interesting that the crystal packing of this β-form is determined by the coordination interaction between the central metal of one molecule and an N atom of a thiadiazole ring of a proximate macrocycle (Fig. 7). As a result, the macrocycles form coordination polymeric zig-zag chains with N–M bond lengths of 2.327, 2.300 and 2.188 Å for the Fe^{II}, Co^{II} and Zn^{II} complexes, respectively. Consecutive macrocycles in the chains form dihedral angles of 83–85° as do the related N–M···N–M bonds.

The observed M–N (axial) distances for the three species are slightly longer than or comparable with that found in the Co^{II} complex with 2,1,3-benzothiadiazole, $[Co(SN_2Bz)Br_2]_n$ (2.208 Å) [40] and definitely longer than for a Cu^{I} complex with 4-methyl-2,1,3-benzothiadiazole $[Cu(SN_2BzMe)I]$ (2.040 Å) [39]. The longer distances are probably a consequence of combined effects due to the different surroundings, oxida-

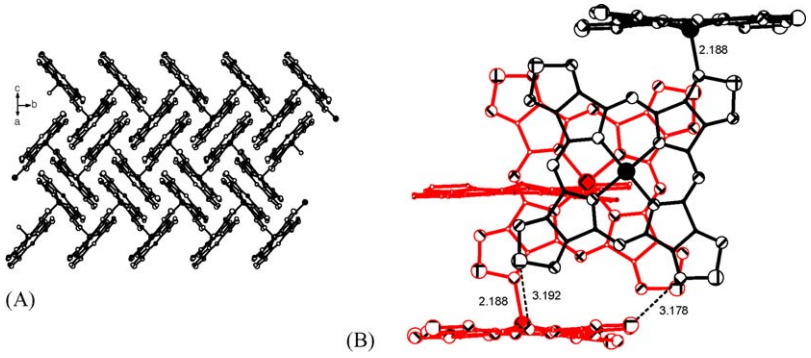

Fig. 7. Molecular packing of β-[TTDPzZn]: (A) coordination polymers along the *b*-axis, (B) molecular overlap between the molecules in adjacent chains. Short N···S contacts are indicated by dashed lines, the corresponding distances are given in Å. Figure produced using data from Ref. [28].

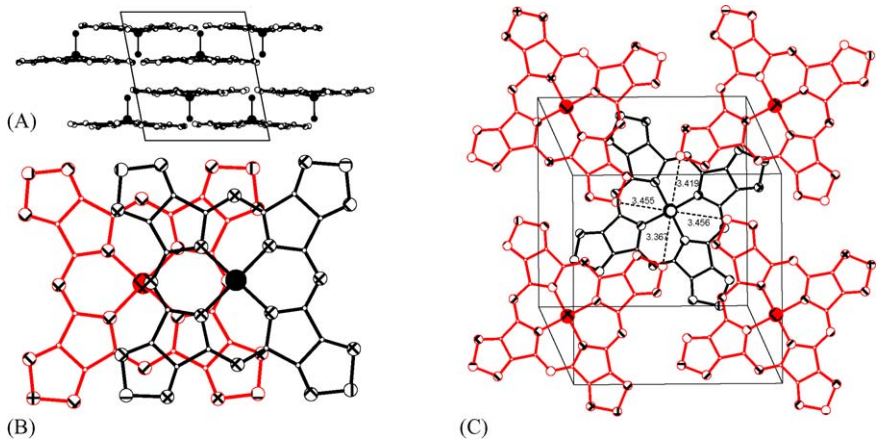

Fig. 8. Molecular packing of [TTDPzAlCl]: (A) view along the *b*-axis, (B) concave–concave overlap, (C) convex–convex overlap. Short N···S contacts are indicated by dashed lines with related distances given in Å. Figure produced using data from Ref. [23].

tion and spin state of the metal ions as well as to the steric requirements of the zig-zag chained arrangement of the macrocycles. Noteworthy, whilst Co^{II} and Fe^{II} ions are in-plane and likely to be involved in strong π-backbonding, the Zn^{II} ion in the β-[TTDPzZn] complex is significantly displaced out of the central N_4 plane of the porphyrazine macrocycle (0.394 Å). The macrocycles in the adjacent chains exhibit a considerable overlap favourable for interplane π–π interaction (Fig. 7B) and, being slipped along the $N_{meso}\cdots N_{meso}$ axis, approach to each other by ca. 3.3 Å. The shortest interplane interatomic contacts are 3.3–3.4 Å. As can be seen from Fig. 7B, van der Waals interactions between S atoms and *meso*- and thiadiazole N atoms (S···N distances ca. 3.1–3.2 Å) also contribute to the attraction of the overlapping polymer chains. Such unique molecular arrangement has not been observed for metal phthalocyanines and endow this crystalline species with peculiar magnetic properties. The magnetic studies [27,28] have shown the antiferromagnetic behavior of β-[TTDPzCo] and β-[TTDPzFe] which was explained in terms of a dimer model.

As shown in Fig. 8A, the two isostructural complexes with tervalent metal ions [TTDPzMCl] (M = Al^{III}, Ga^{III}), indicated here as α_2 polymorphs (Table 4), have a molecular packing consisting of stacked double layers [23]. The metal centers are five coordinated and displaced out of the central N_4 cavity (Al^{III}, 0.416(6) Å; Ga^{III}, 0.448(6) Å) towards the Cl^- ion.

As seen in Fig. 8C, the arrangement of the macrocycles within a double layer (convex–convex overlap) shows the axial chloride of a macrocycle of the bottom layer at a van der Waals distance (ca. 3.4 Å) from the S (and N) atoms of four macrocycles of the top layer. The short interplane interatomic contacts in a double layer are 3.3–3.4 Å and the distance between the mean planes of the molecules is ca. 3.2 Å. However, interplane overlap of the macrocycles is almost absent and π–π interaction within a double layer is hardly possible. In contrast to that, the neighbouring molecules in the adjacent double layers exhibit the significant concave–concave overlap with slipping along the $N_{meso}\cdots N_{meso}$ axis (Fig. 8B) similar to that observed in γ-polymorph of the Cu^{II} and Ni^{II} complexes. This facilitates the interplane π–π interaction and the shortest interatomic distances between overlapping adjacent molecules reach values of 3.1–3.2 Å.

As has just been illustrated, progressive annulation of thia/selenodiazole heterocycles to the porphyrazine macrocycle and the type of incorporated metal centers have a large impact on the molecular arrangement with formation of highly diversified crystal packing patterns. In going from a "S-porphyrazine" to the corresponding "Se-porphyrazine", the structural features are maintained essentially unchanged as can be verified by comparing the low-symmetry "Se-porphyrazine" **20a** with the corresponding isomorphous S-analogue **15a** (see Fig. 2).

The Mg^{II} complex of hexapropyl substituted selenodiazoloporphyrazine **26b**, in a way similar to what is observed for monoannulated free-bases **15a** and **20a**, forms a centrosymmetric face-to-face molecular pair (Fig. 9) [29]. In this case, the formation of a dimer is also determined by hydrogen bonding of the water molecule coordinated to the fifth position of the Mg^{II} ion in one macrocyclic unit with *meso*- and selenodiazole N atoms of another closely lying unit (H···N distances are 1.939 and 2.294 Å, respectively). Moreover, the selenodiazole ring of one molecule and the pyrrole ring of the other within the pair mutually overlap with shortest intermolecular atom–atom contacts of 3.3–3.4 Å. The dimer pairs are arranged into back-to-back stepped stacks in which the Se atom of one dimeric unit is located above the pyrrolic N atom of another with Se···N distance of 3.411 Å and the distance between two C_α atoms is 3.373 Å.

3.2. Geometrical features

From the huge amount of available X-ray data on the octaamyloxyphthalocyanine [$(AmO)_8PcH_2$] and the series of low-symmetry and symmetrical macrocycles with incorporated thia/selenodiazole rings, it is evident that the bond lengths of the porphyrazine core are only minimally affected (Table 5) upon progressive substitution of the benzene rings by annulated thia/selenodiazole rings. One can only notice a small (0.01 Å), although systematic, contraction of the N_{meso}–C_α bonds and elongation of C_α–$N_{pyr}H$ bonds. More consistent is instead the variation seen of the bond angles. Table 5 shows that the angles $\angle C_\alpha(N_{pyr}H)C_\alpha$ in the pyrrole rings are increased by 3–4° and the angle $\angle N_{meso}C_\alpha N_{pyr}$ by 1–2° with the increasing presence of the

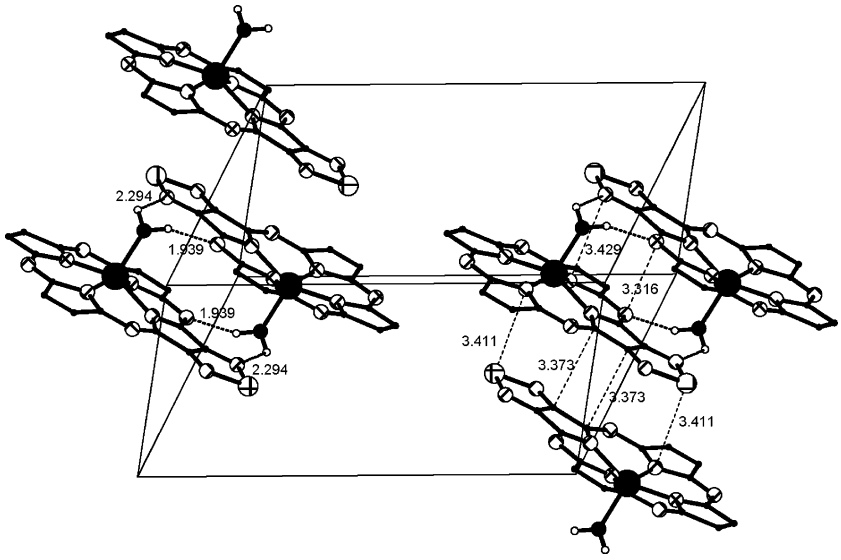

Fig. 9. Crystal and molecular structure of $[Pr_6SePzMg(H_2O)]_2$ [29]. Propyl chains are not shown. Figure produced using data from Ref. [29].

thiadiazole rings. As a result, an expansion is determined of the central coordination cavity with respect to that of the phthalocyanine macrocycle. In fact, the measured distances between internal opposite N_{pyr} atoms are 3.910 and 3.953 Å for $[PcH_2]$ [54], which become 3.952 and 4.062 Å for $[TTDPzH_2]$ [27].

A similar expansion of the central hole is observed for the metal complexes, [TTDPzM] and [TTDPzMCl], when comparison is made with the corresponding metallophthalocyanines β-[PcCu] [55], β-PcFe [56], β-[PcCo] [57], β-[PcZn] [58], [PcAlCl] [59], [PcGaCl] [59,60] (see Table 6). Such enlargement of the central hole in the TTDPz macrocycle must be related to the fact that annulation of the five-membered thiadiazole ring to the pyrrole ring stresses the angle $C_\alpha C_\beta N_{het}$ (Fig. 10) more than in the case of annulation of the six-membered benzene ring, thus producing the observed modifications.

The influence of the thiadiazole annulation on the geometry of the porphyrazine macrocycle has also been examined in two theoretical studies in which geometry was optimized using an

Table 5
Average geometric parameters of the macrocyclic skeleton in porphyrazines with annulated 1,2,5-thia/selenodiazole and/or benzene rings[a]

Geometric paramater	$[(AmO)_8PcH_2]$ (**19**)	$[SeA_3PzH_2]$ (**20a**)	$[SA_3PzH_2]$ (**15a**)	$[S_2A_2PzH_2]$ (**17a**)	$[TTDPzH_2]$ (**5**)	$[PcH_2]$
C_α–N_{meso}	1.330	1.325	1.326	1.322	1.321	1.327
C_α–N_{pyr}	1.371	1.376/1.370	1.372/1.367	1.373/1.365	1.371	1.373
C_α–$N_{pyr}H$	1.373	–/1.371	–/1.372	1.368/1.370	1.382	1.373
C_α–C_β						
(N)	1.466	1.445/1.445	1.447/1.448	1.451/1.455	1.465	1.461
(NH)	1.451	–/1.469	–/1.460	1.458/1.443	1.447	1.452
C_β–C_β						
(N)	1.401	1.434/1.424	1.410/1.416	1.395/1.413	1.400	1.395
(NH)	1.409	–/1.394	–/1.393	1.394/1.412	1.408	1.398
$N_{pyr}\cdots N_{pyr}$	3.854	3.852	3.860	3.920	3.952	3.910
$N_{pyr}H\cdots N_{pyr}H$	4.067	4.101	4.097	4.043	4.062	3.953
N_{pyr}–$N_{pyr}H$	2.749	2.737	2.748	2.781	2.837	2.721
	2.853	2.888	2.880	2.849	2.830	2.837
N_{pyr}–H	0.820	–/1.018	–/1.000	1.001/0.949	0.891	0.923
$H\cdots N_{pyr}$	2.203	2.135	2.140	2.186	2.277	2.101
	2.352	2.251	2.260	2.261	2.286	2.343
$\angle C_\alpha N_{meso} C_\alpha$	122.8	120.7	121.1	122.5	123.5	121.8
	124.3	125.2	125.5	124.7	123.6	123.6
$\angle C_\alpha N_{pyr} C_\alpha$	106.9	110.1/107.3	109.7/107.3	109.7/107.5	108.7	108.0
$\angle C_\alpha(N_{pyr}H)C_\alpha$	111.8	–/111.8	–/111.7	114.4/109.9	113.6	109.7
$\angle N_{meso} C_\alpha N_{pyr}$	127.1	129.9/127.7	129.6/128.4	128.8/127.7	128.3	127.9
$\angle N_{meso} C_\alpha N_{pyr}H$	128.3	–/127.7	–/127.4	130.1/127.0	129.3	128.2

[a] For the low symmetry species the average data are given for thia(seleno)diazole/benzene annulated non-equivalent pyrrole and pyrrolenine rings.

Table 6
Comparison of the selected geometric parameters in metal complexes of [$TTDPzH_2$] and [PcH_2]

Complex	M–N	$\angle N_{pyr}C_\alpha N_{pyr}$	M–C_t	N–C_t	Ref.
α-[TTDPzNi]	1.923	108.1			[28]
γ-[TTDPzNi]	1.928	108.3			[28]
[PcNi]					
α′-[TTDPzCu]	1.972	109.8			[28]
γ-[TTDPzCu]	1.968	109.5			[28]
[PcCu]					[55]
β-[TTDPzFe]	1.957	109.0	0		[28]
β-[PcFe]	1.926	107.3	0		[56]
β-[TTDPzCo]	1.942	108.9	0		[27,28]
β-[PcCo]	1.920	107.0	0		[57]
β-[TTDPzZn]	2.044	110.6	0.394		[28]
β-[PcZn]	1.980	109.1	0		[58]
[TTDPzAl(Cl)]	2.000		0.416	1.96	[23]
[PcAl(Cl)]	1.98		0.410	1.94	[59]
[TTDPzGa(Cl)]	2.012		0.444	1.962	[23]
[PcGa(Cl)]	1.983		0.439	1.93	[59,60]

AM1 method [61] and a DFT approach with B3LYP/6-31G(d) basis set [32]. Although quantum chemical modeling of the geometrical structure of the isolated molecule in a gas phase somewhat overestimates the bond lengths as compared with the data from the X-ray single crystal study, they reproduce the effect of expansion of the porphyrazine macrocycle due thiadiazole ring annulation.

On the basis of X-ray studies the position of the inner hydrogen atoms in the free-bases **15a**, **17a** and **20a** has been located [20,21]. The NH groups are seen in opposite pyrrole rings and their H atoms form hydrogen bonds with the N atoms of the adjacent pyrrolenine rings. The $N_{pyr}H\cdots N_{pyr}$ distances of 2.13–2.35 Å are considerably shorter than the sum of the van der Waals radii of N and H atoms (1.55 + 1.20 Å). According to single crystal X-ray data [20], compounds **15a** (Fig. 2) and **20a** (Fig. 11), bearing three diamyloxybenzene fragments and one thia- or selenodiazole ring, exist in the solid state as 22*H*,24*H* tautomers, in which the NH groups belong to two opposite isoindole units with concomitant facing of the thia/selenodiazole ring with the isoindolenine fragment. The semiempirical AM1 calculations [24] of the model compound without amyloxy substituents have shown that this 22*H*,24*H*-tautomer is more stable by 17.5 kJ/mol than the alternative 21*H*,23*H*-tautomer having two opposite isoindolenine units and benzene and thiadiazole rings annulated to two opposite pyrrole rings.

The variable temperature ^{1}H NMR data obtained for **15a** in $CDCl_3$ in the temperature range from 20 to −50 °C [21] also

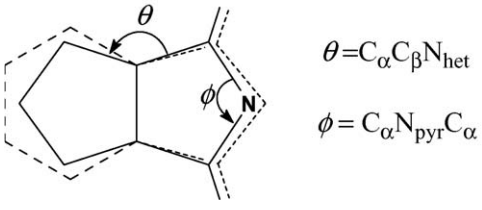

Fig. 10. Effect of 5–5 vs. 5–6 ring fusion on the geometry of the pyrrole rings in annulated porphyrazines.

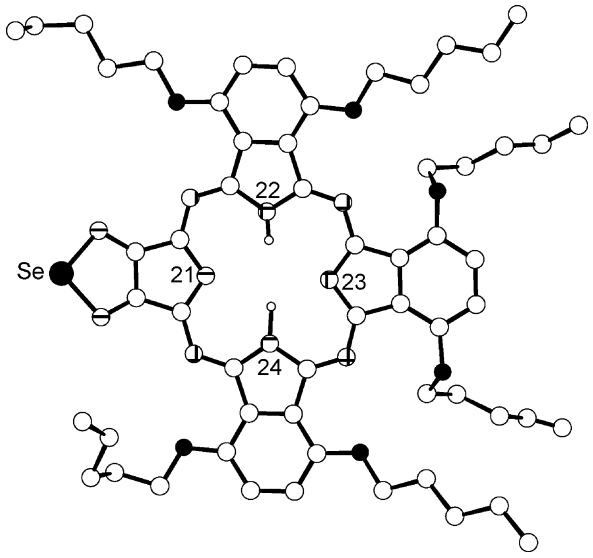

Fig. 11. Molecular structure of **20a** in the form of the 22*H*,24*H* tautomer. Figure produced using data from Ref. [20].

provide evidence for the presence of the 22*H*,24*H*-tautomer and show the absence of tautomerism with formation of the 21*H*,23*H* tautomer. This is unlike the situation observed for **17a**, when rapid NH tautomerism of two unequivalent NH groups at ambient temperatures results in a single NH resonance, whereas two signals are shown below −40 °C (Fig. 12).

The geometry of the 1,2,5-thiadiazole and 1,2,5-selenodiazole fragments annulated by the porphyrazine macrocycle is similar to that found in other compounds containing these heterocyclic units, e.g. for 2,1,3-benzothia- and 2,1,3-benzoselenodiazoles (SN_2)Bz and (SeN_2)Bz [62] (Table 7). No substantial difference is observed for the bond lengths and bond angles for thiadiazole rings annulated to pyrrole and pyrrolenine fragments of the porphyrazine macrocycle in **5** and **17a**. The geometrical parameters of annulated thia/selenodiazole rings obtained from X-ray work are crucial for the correct conclusions to be drawn about the electronic structure of these fragments and the macrocycle as a whole.

3.3. Electronic structure

Annulation of thia- or selenodiazole rings to the porphyrazine macrocycle creates a very peculiar electronic situation which cannot be correctly depicted with any of the classical resonance structures containing single and double bonds shown in Chart 4(**A**–**E**) and involving the sulfur atoms in the oxidation states +2 (**A**) and +4 (**B** and **C**) and in *meso*-ionic structures (**D** and **E**).

The analysis of the numerous structural data on relatively simple organic compounds containing the 1,2,5-thiadiazole ring [62,63] and results of their quantum chemical investigations [64–67] have shown that none of the structures **A**–**E** (Chart 4) can individually explain the structural and chemical properties of these species. It was concluded [62,66] that the real aromatic structure is best depicted by the representation **F**, mainly contributed by structures **A** and **D**, with minor participation of the others (**B**, **C**, and **E**). Accordingly, the X-ray data obtained for

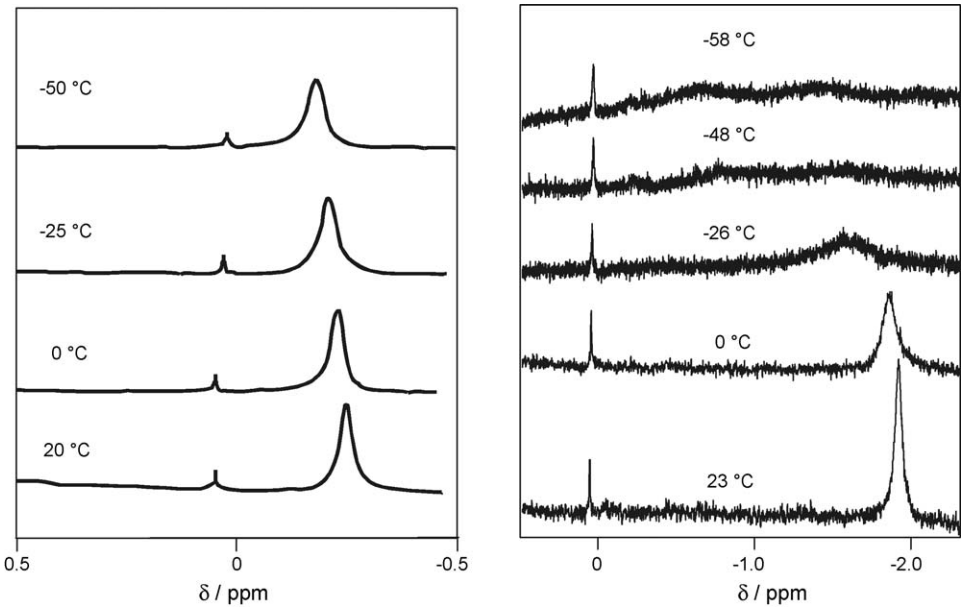

Fig. 12. ^{1}H NMR spectra of **15a** (left) and **17a** (right) in $CDCl_3$ [21].

Table 7
Geometrical parameters of annulated 1,2,5-thia- and 1,2,5-selenodiazole rings

	$(SN_2)Bz$	$[TTDPzH_2]$ (**5**) N/NH	$[S_2A_2PzH_2]$ (**17a**) N/NH	$[SA_3PzH_2]$ (**19a**)	$[SeA_3PzH_2]$ (**20a**)	$(SeN_2)Bz$
X–N	1.60	1.647/1.631	1.631/1.633	1.633	1.807	1.83
N–C	1.34	1.326/1.328	1.329/1.334	1.311	1.304	1.30
C_β–C_β	1.41	1.400/1.408	1.395/1.394	1.410	1.434	1.46
∠N–X–N	102	100.5/101.3	100.6/101.9	101.9	96.5	95
∠X–N–C_β	105	104.5/104.6	104.9/103.7	103.6	102.8	104
∠N–C_β–C_β	114	115.3/114.7	114.8/115.4	115.5	118.8	118
Ref.	[62]	[27]	[21]	[20]	[20]	[62]

tribenzoporphyrazines **15a** and **20a** containing one annulated thia/selenodiazole ring [20,21] allow to propose structure **G** for the macrocycle (Chart 4) in which the annulated heterocycle is represented as in **F**.

The bonds in the annulated thiadiazole ring in **15a** (S–N (1.633 Å), N–C (1.311 Å) and C–C (1.410 Å) [20]) are intermediate between those expected for single (S–N, 1.74 Å, N–C, 1.47 Å and C–C 1.54 Å) and double bonds (S=N, 1.56 Å, N=C, 1.29 Å and C=C 1.33 Å). Assuming the typical lengths for S–N and S=N bonds, calculation of the bond order (N_{SN}) for the thiadiazole ring in **15a** by using the formula [68]:

$$N_{SN} = \frac{12.407}{(l_{SN})^2} - 3.098$$

leads to an N_{SN} value of 1.55, a value requiring participation of structure **D**. However, the CN bond lengths have high double bond character (for **15a** $N_{CN} = 1.77$, and for the Se-analogue **20a** $N_{CN} = 1.81$) which calls for the involvement of structure **A**. In

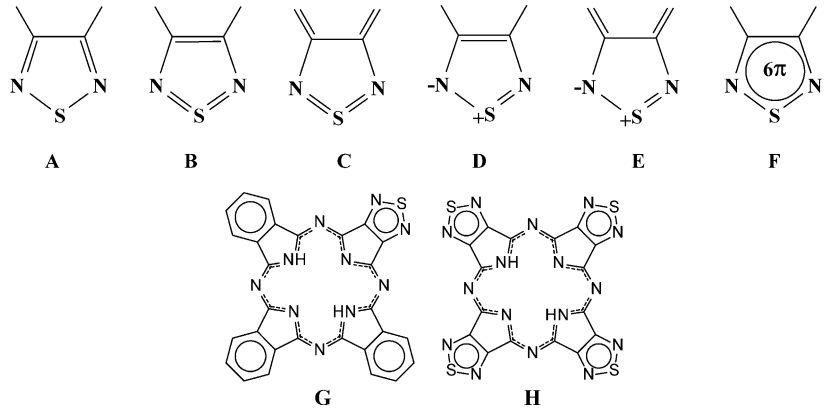

Chart 4.

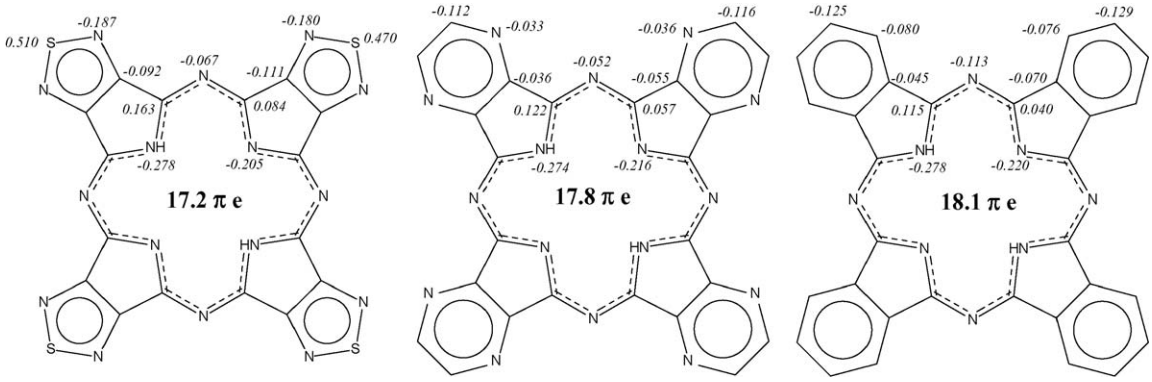

Fig. 13. The atomic charges in porphyrazines with annulated 1,2,5-thiadiazole, pyrazine and benzene rings and the net π-electron population of the atoms constituting the internal 16-membered ring calculated by the AM1 method.

conclusion, then, structure **F** for the thiadiazole ring is the adequate representation in the macrocycle **15a** (**G**, Chart 4), and is as well representative for the macrocycles **20a** [20,21] and **26b** [29] in which Se replaces the S atom. The angle formed by the chalcogen atom in the thia/selenodiazole ring of **15a** (∠NSN = 101.9°) and **20a** (∠NSeN = 96.5°) indicates that σ-bonding with neighbouring N atoms mainly implies participation of np_x and np_y orbitals ($n = 3$ for S and 4 for Se). One of the lone pairs is mainly localized on the n*s* orbital, whilst the other one is located on the np_z orbital and is highly involved in the conjugated π system of the entire macrocycle.

Semiempirical AM1 calculations [24,26] support the above proposed electronic structure for the thiadiazole fragment. The population of the S atom orbitals is for 3s 1.852, for $3p_x$ and $3p_y$ 1.245 and for $3p_z$ 1.260 electrons. Delocalization of electrons from the $3p_z$ orbital leads to considerable positive charge on the S atom ($\delta = 0.435$), which is in agreement with a substantial contribution of the *meso*-ionic structure **D** and scarce participation of the structures **B** and **C** with S^{IV} having 3d orbitals involved. The negative charge on the N atoms of the thiadiazole rings $\delta = -0.187$ appears as due to excessive π-charge (population of the $2p_z$ orbital is 1.19–1.20), and the lone pair has a considerable *s*-character (population of the 2s orbital is 1.758), leading to the low basicity of these N atoms (see Section 4.1.2 below).

In the case of tetrakis(thiadiazole)porphyrazine, [$TTDPzH_2$], carrying four thiadiazole rings each one hypothetically involving resonance structures **A**–**E** (Chart 4), the possible number of macrocyclic resonance structures becomes very large. However, for this macrocycle the delocalized structure **H** (Chart 4), which was proposed by us in our first paper [14], can be considered as the most correct depiction of the electronic situation in the molecule, in full agreement with recent X-ray [27] and theoretical data [32,61].

The results of calculations [61] show that annulation of thiadiazole rings has considerable influence on the distribution of the electron density in the porphyrazine macrocycle. This influence is more marked than the annulation of the pyrazine rings which are often considered [63] to have a similar electronic effect as the 1,2,5-thiadiazole rings. Thus the positive charge on the C_α-atoms and the π-deficient character of the internal 16-membered macrocycle increase in the order [PcH_2] < [$(Pyz)_4PzH_2$] < [$TTDPzH_2$] (see Fig. 13), a relative measure of the strong σ- and π-acceptor influence of 1,2,5-thiadiazole fragments. This is also in agreement with the recent electrochemical study [23] which demonstrates that the TTDPz macrocycle in the Al^{III}, Ga^{III} and In^{III} complexes [TTDPzMX] (X = Cl, OH or AcO) is much more easily reduced (by 0.4–0.5 V) than the Pc macrocycle in the corresponding [PcMX] complexes (see below Table 13 in Section 5), but unlike the latter species could not be oxidized.

The semiempirical ZINDO/S calculations [26,69] demonstrate that annulation of four thiadiazole rings in [$TTDPzH_2$] leads to stronger stabilization of the frontier orbitals as compared to [PcH_2] than in the case of the pyrazine annulation in [$(Pyz)_4PzH_2$] (see Fig. 14). On the contrary, 3,4-annulation of four thiophene rings leads to destabilization of all frontier π-MOs, especially of the HOMO, suggesting that tetrakis(3,4-thiopheno)porphyrazine, [$(^{3,4}Th)_4$}PzH_2], should be unstable due to the high reactivity of the thiophene rings in side reactions. Indeed, all attempts to prepare these species were unsuccessful [5,9,12] and in mono(3,4-thiopheno)porphyrazines, so far the only species reported [9,10], the thiophene ring is easily involved

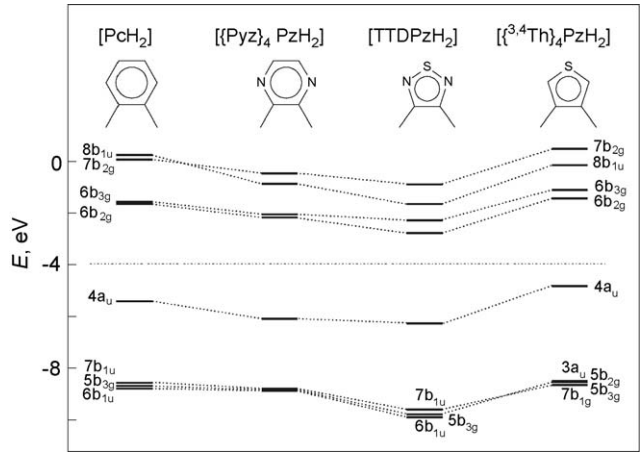

Fig. 14. MO diagram of porphyrazines with annulated heterocycles based on ZINDO/S calculations on the AM1/UHF optimized structures [69].

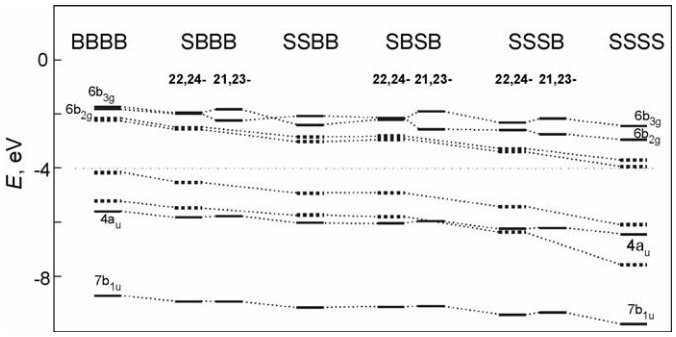

Fig. 15. Influence of the progressive substitution of benzene rings in phthalocyanine (BBBB≡[PcH_2]) by thiadiazole rings (SSSS≡[$TTDPzH_2$]) on the energies of the frontier π-MOs calculated by the ZINDO/S method for AM1 optimized structures [26,69]. MO levels for porphyrazines with 3,6-dimethoxy substituted benzene rings calculated by the DFT method [32] are indicated by dashed lines.

in a Diels-Alder type reaction with dienophiles [10]. Therefore, the introduction of two N atoms into the 3,4-annulated thiophene ring appears to be a crucial factor determining the observed stability of tetrakis(thiadiazole)porphyrazines.

The effect of the progressive substitution of the benzene rings or 3,6-dimethoxybenzene rings annulated to the porhyrazine core by thiadiazole fragments on the energies of the frontier π-MOs has been studied by ZINDO/S [26,69] and DFT [32] methods. Similar trends are shown for both systems. In fact, when benzene moieties in [PcH_2] or in its octamethoxy derivative [$(MeO)_8PcH_2$] are progressively replaced by thiadiazole fragments, the four frontier orbitals are stabilized in the series of BBBB (≡[PcH_2] or [$(MeO)_8PcH_2$]), SBBB, SBSB, SSBB, SSSB and SSSS (≡[$TTDPzH_2$]) (Fig. 15).

According to ZINDO/S results [26,69], if two different NH tautomers are possible, as is the case for SBBB, SBSB and SSSB macrocycles (Chart 5), the HOMOs have lower energy

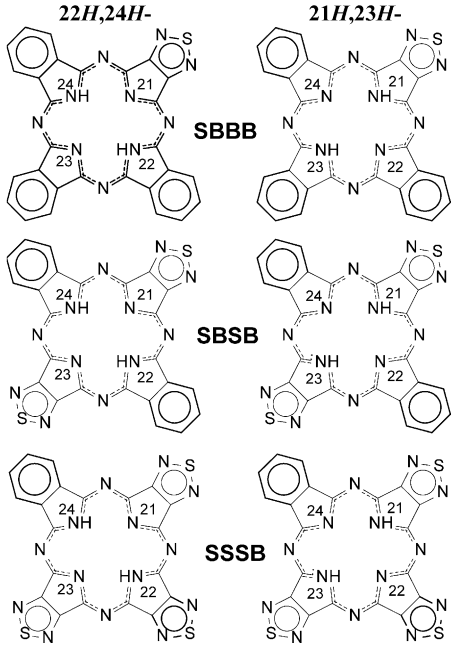

Chart 5.

for tautomers of type 22*H*,24*H* which have a larger number of the isoindole fragments (2, 2 and 1, respectively). The 21*H*,23*H* tautomers with larger number of isoindolenine units have higher energies of HOMO and, hence, they are less stable than the corresponding 22*H*,24*H* tautomers. One thiadiazole ring located along the NH···NH axis in 21*H*,23*H* tautomers destabilizes the molecule by 4.1 kcal/mol in the respect to the 22*H*,24*H* tautomer. Two NH tautomers differ also in the relative position of LUMO and LUMO + 1 since the observed splitting of these orbitals is considerably less for the 22*H*,24*H* tautomer.

4. Spectroscopic properties

Annulation of thia/selenodiazole rings to the porphyrazine core highly influences the electronic and vibrational states of the present "S- and "Se-porphyrazines". This will be shown in this section by examining the effects produced by such annulation on the linear and non-linear optical properties and vibrational spectra.

4.1. UV/visible spectra

The UV/visible solution spectra of the symmetrical free-bases [$TTDPzH_2$] and [$TSeDPzH_2$], their metal derivatives and all related low-symmetry species have a spectroscopic pattern which is typical for porphyrazine-type macrocycles and consists of the presence of intense absorptions due to intraligand π–π^* transitions in the Soret (300–400 nm) and Q band (600–800 nm) regions. The Soret band is usually broadened since it originates from the configuration interaction of several closely lying π–π^* transitions and underlying n–π^* transitions involving the N atoms of the porphyrazine macrocycle and annulated thia/selenodiazole rings. The Q absorption in porphyrazines originates from the pure π–π^* transitions from the HOMO to LUMO and LUMO + 1 energy levels in accordance with Gouterman model [70]. The shape and peak position of the absorption bands are determined by the number and location of annulated thia/selenodiazole rings and by the presence and type of metal center. Moreover, strong solvatochromic effects are observed as it will be shown by the data in neutral, basic and acidic solvents.

4.1.1. Neutral solvents

As already demonstrated in Section 2.1, the symmetrical free-bases [$TTDPzH_2$] and [$TSeDPzH_2$] and their metal derivatives, like their phthalocyanine analogues, are almost insoluble in non-donor solvents (chlorobenzene, dichloromethane, etc.) and only qualitative spectra can be obtained. Table 8 summarizes the spectroscopic data for the free-bases [$TTDPzH_2$] and [$TSeDPzH_2$], their Mg^{II} complexes and related species. Tables 9 and 10 list the data for the TTDPz and TSeDPz metal derivatives.

For [TTDPzM] and [TSeDPzM] as well as for the phthalocyanine and porphyrazine analogues, [PcM] and [PzM], due to the effective D_{4h} symmetry of their π-chromophore, the LUMO and LUMO + 1 are degenerate and a single sharp Q band with vibronic satellites on the blue side is observed in neutral and basic solvents as is exemplified in Fig. 16 for the series of Mg^{II} complexes in pyridine solution. For the corresponding free-

Table 8
UV–visible solution spectra of free-base and Mg^{II} tetrakis(thia/selenodiazole)porphyrazines and related porphyrazines

Porphyrazine	Solvent	λ_{max} (nm) (log ε)						Ref.
		Free-base			Mg^{II} complex			
		Soret	Q_y	Q_x	Soret	Q_{vib}	Q	
[PzH_2]	PhCl	333 (4.70)	545 (4.60)	617 (4.75)				[72]
	Py	333 (4.79)	542 (4.57)	613 (4.71)	332 (4.70)	535 (4.14)	587 (5.07)	[69]
[PcH_2]	ClNP[a]	350 (4.74)	665 (5.18)	698 (5.21)		611 (4.08)	680 (4.93)	[71]
	Py		659	694	347 (4.73)	610 (4.45)	675 (4.94)	[71]
[$(pyz)_4PzH_2$]	ClNP		625	660				[73]
	DMSO		580sh	635		580sh	635	[73]
[$TTDPzH_2$]	PhCl	333	641	653	330	590sh	647	[14]
	py	375 (4.53)	622sh	648 (4.71)	371 (4.51)	585 (4.00)	642 (4.85)	[14]
[$TSeDPzH_2$]	py	382 (4.56)	650sh	682 (4.65)	356 (4.31)	618 (3.77)	674 (4.38)	[16]

[a] ClNP, 1-chloronaphthalene.

Table 9
UV/visible spectroscopic data of the metal derivatives of tetrakis(thiadiazole)porphyrazine [14,15,23]

[TTDPzM]		λ (nm)							
M	Solvent	Soret region			CT region		Q region		
Zn^{II}	Py	336	367	396sh			588	619	645
	DMSO	329	353	398sh			585	609sh	638
	CF_3COOH	327					583	613sh	643
	H_2SO_4	323					603	632sh	664
Cu^{II}	PhCl	337					584	618	642
	Py	331	363sh		439		586	618	642
	CF_3COOH	275	325	395sh	457sh		575	609sh	631
	H_2SO_4	270	306sh	322			598sh	627sh	661
Ni^{II}	Py	311	327sh	365			578	605sh	631
	DMSO	305		358			571	603	627
	CF_3COOH	322		390sh			576sh	597sh	635
	H_2SO_4	317					601	627sh	660
Co^{II}	Py	341			445		585sh	605sh	639
	DMSO	331			458		580sh	605sh	632
	CF_3COOH	315					578sh	602sh	632
	H_2SO_4	314					593sh	631sh	656
Fe^{II}	Py	344		411	443	504	603sh	646sh	676
	CF_3COOH	320			472	577sh	599sh	627sh	643
	H_2SO_4	306			481			667sh	693
Mn^{II}	DMSO	309	352sh	375sh	466sh	498sh	599sh	623sh	653
	CF_3COOH	330			513		593sh	618sh	646
	H_2SO_4	316sh	384sh				601sh	642sh	662
$Al^{III}Cl$	py	340	364sh	393sh			590	622	647
	DMSO	340					590	623	649
	CF_3COOH	329					583	620	
	H_2SO_4	330					600sh	649sh	660
$Ga^{III}Cl$	py	337	367sh	400sh			585	617	645
	DMSOa	338					587	624	647
	CF_3COOH	329					582	615	640sh, 645
	H_2SO_4	330					597sh	648sh	659
$In^{III}OAc$	py	321	365sh	390sh			602		658
	DMSO	357sh					609	636sh	658
	CF_3COOH	328	371sh				594	629	646, 652sh
	H_2SO_4	317	390sh				618sh		670

Table 10
UV/visible spectroscopic data of the metal derivatives of tetrakis(selenodiazole)porphyrazine [16,17]

[TSeDPzM]		λ (nm)								
M	Solvent	Soret region			CT region			Q region		
Zn^{II}	Py	313		360				626	652	681
	DMSO	320		353				626	659	680
	CF_3COOH		340					610	641	667
	H_2SO_4	256	332	361				607	645	699
Cu^{II}	Py	321sh		361				627sh	651sh	677
	H_2SO_4			355				611	652	705
	CF_3COOH	305								662
Ni^{II}	ClNP		356		424			620	656	686
	Py			357				604	631	661
	DMSO		353					602	631	657
	CF_3COOH	311						610	640	669
	H_2SO_4		335	358				601	638	693
Co^{II}	ClNP		358		438	469	497	620	655	687
	Py		334	352	396	441	473	606	645	673
	DMSO		331sh	347		476		609		670
	CF_3COOH	319						598	631	664
	H_2SO_4		344		430	499	604	641	667	700
Mn^{II}	DMSO		347		445				626	685
	CF_3COOH	283, 294	305	339				537	613	668
	H_2SO_4		341				625	657	682	709

bases, the symmetry is lowered to D_{2h}, the degeneracy of LUMO is lifted and a double-peaked Q band containing Q_x and Q_y components is observed as shown in the series of spectra recorded in chlorobenzene (Fig. 17).

The Q band region in porphyrazines is generally highly sensitive to the type of substitution or annulation. When four thia/selenodiazole rings are fused to the central porphyrazine core, the macrocyclic 26π electron chromophore present in

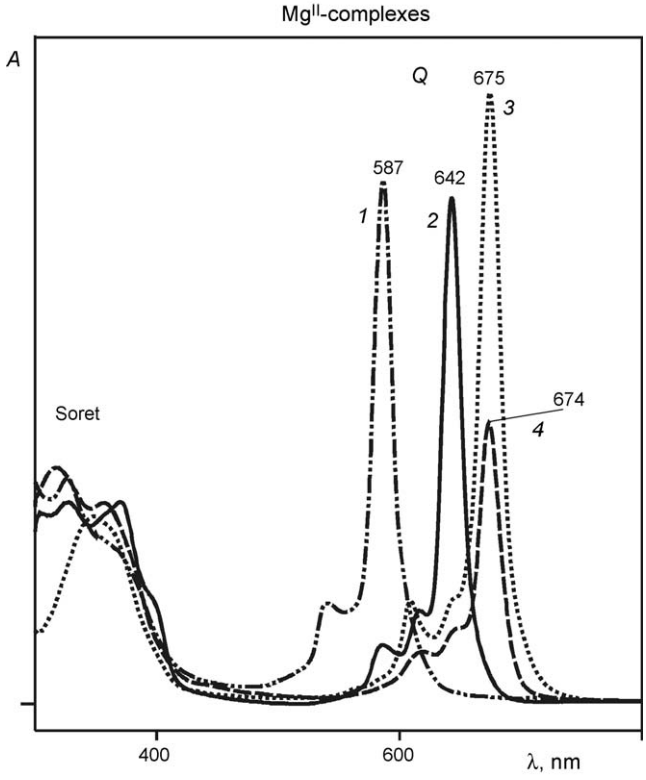

Fig. 16. UV/vis spectra of [PzMg] (1), [TTDPzMg(H_2O)] (2), [PcMg] (3) and [TSeDPzMg(H_2O)] (4) in pyridine.

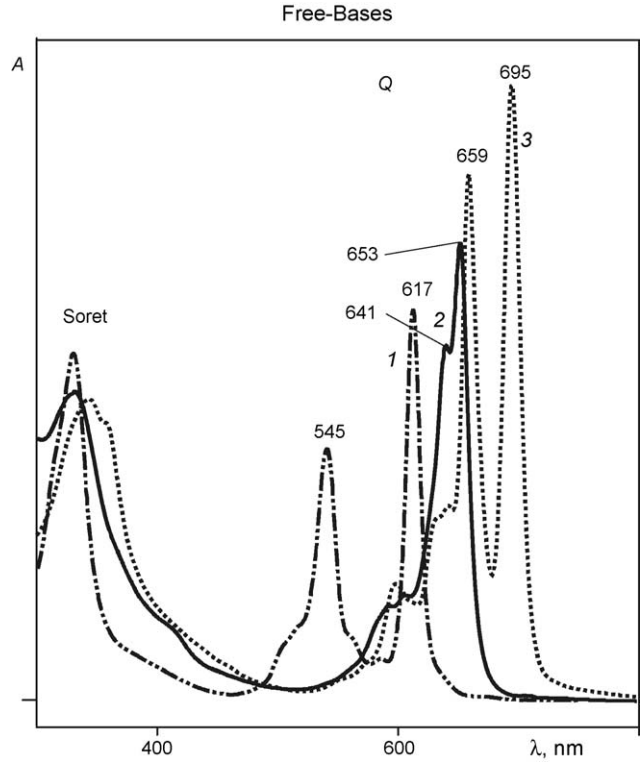

Fig. 17. UV/vis spectra of [PzH_2] (1), [$TTDPzH_2$] (2) and [PcH_2] (3) in chlorobenzene.

unsubstituted porphyrazine [PzH_2] and its metal complexes [PzM] is extended to the 42π-electron chromophoric system in [TTDPzM] and [TSeDPzM]. Such a π-extension results in a considerable bathochromic shift of the Q band maxima, similarly to what is observed for the benzene or pyrazine annulation in formally π-isoelectronic phthalocyanines [PcM] and tetrapyrazinoporphyrazines [{Pyz}$_4$PzM]. As shown in Figs. 16 and 17, the Q band which is observed at 587 nm for [PzMg] and at 617 nm (Q_x) and 545 nm (Q_y) for [PzH_2] in the case of thiadiazole annulation is bathochromically shifted to 642 nm for [TTDPzMg(H_2O)] ($\Delta\lambda(Q) = 55$ nm (1460 cm^{-1})) and to 653 and 641 nm for [$TTDPzH_2$] ($\Delta\lambda(Q_x) = 36$ nm (890 cm^{-1}) and $\Delta\lambda(Q_y) = 96$ nm (2750 cm^{-1}). The value of the bathochromic shift is substantially smaller than in the case of benzene annulation in [PcMg] ($\Delta\lambda(Q) = 88$ nm (2220 cm^{-1})) and in [PcH_2] ($\Delta\lambda(Q_x) = 78$ nm (1880 cm^{-1}) and $\Delta\lambda(Q_y) = 114$ nm (3270 cm^{-1})). The observed effect of thiadiazole rings is similar to the effect of pyrazine rings in [(Pyz)$_4$PzMg] ($\Delta\lambda(Q) = 48$ nm (1290 cm^{-1}) and in [(Pyz)$_4$$PzH_2$] ($\Delta\lambda(Q_x) = 43$ nm (1060 cm^{-1}) and $\Delta\lambda(Q_y) = 80$ nm (2350 cm^{-1}) [73], Table 8). This indicates that the thiadiazole ring as well as the pyrazine ring exhibit a π-deficient character in agreement with the observed redox behavior [23] (Section 5) and MO calculations [26,69] (Section 3.3). The bathochromic effect of selenodiazole annulation in [TSeDPzMg(H_2O)] ($\Delta\lambda(Q) = 87$ nm (2200 cm^{-1})) is larger than that of thiadiazole rings and comparable with the effect of benzene annulation (Table 8; Fig. 16). This is explained by the difference in electronegativity of the Se and S atoms and less effective $4d_\pi$(Se)–$2p_z$(N) interaction than $3d\pi$(S)–$2p_z$(N) interaction.

As regard to low-symmetry porphyrazines, the symmetry of the π-chromophore is lower than D_{4h} and a double Q band is observed both for the free-bases and metal complexes (Fig. 18), unless LUMO and LUMO + 1 are occasionally degenerate (e.g. [S_2B_2PzMg] (**22b**) see Fig. 19).

Available spectroscopic data on low-symmetry thia/selenodiazoloporphyrazines and related species (Table 11) allow the analysis of the spectroscopic changes as a function of type of annulation. Thus, when two β-phenyl groups in β-octaphenylporphyrazine, [Ph_8PzH_2] [74], are substituted by one annulated thiadiazole, selenodiazole or benzene ring as in [Ph_6SPzH_2] (**23a**), [Ph_6SePzH_2] (**24a**) and [Ph_6BzPzH_2], [46] the long wave Q_x band is shifted bathochromically from 663 to 682, 693 and 691 nm, respectively ($\Delta\lambda(Q_x) = 19$, 30 and 28 nm (420, 650 and 610 cm^{-1}). Substitution of two β-propyl groups in β-octapropylporphyrazine, [Pr_8PzH_2], by one annulated selenodiazole ring in [Pr_6SePzH_2] (**26a**) induces a bathochromic shift from 627 to 653 nm ($\Delta\lambda(Q_x) = 26$ nm (635 cm^{-1}), whilst fusion of a dimethylpyrazine fragment in [Ph_6(Me$_2$Pyz)PzH_2] leads only to a 7 nm shift (180 cm^{-1}) [29,31].

It is remarkable that substitution of one benzene moiety in tetra(*tert*-butyl)phthalocyanine, [(^{t}Bu)$_4$$PcH_2$] [75], by one π-deficient thiadiazole ring in [SB_3PzH_2] (**21a**) leads to a hypsochromic shift of the Q_x band maximum from 699 to 693 nm ($\Delta\lambda(Q_x) = 6$ nm (200 cm^{-1}), whereas introduction of one π-excessive thiophene ring in [(^{3,4}Th)B_3PzH_2] leads to a bathochromic shift to 727 nm ($\Delta\lambda(Q_x) = 28$ nm (550 cm^{-1})

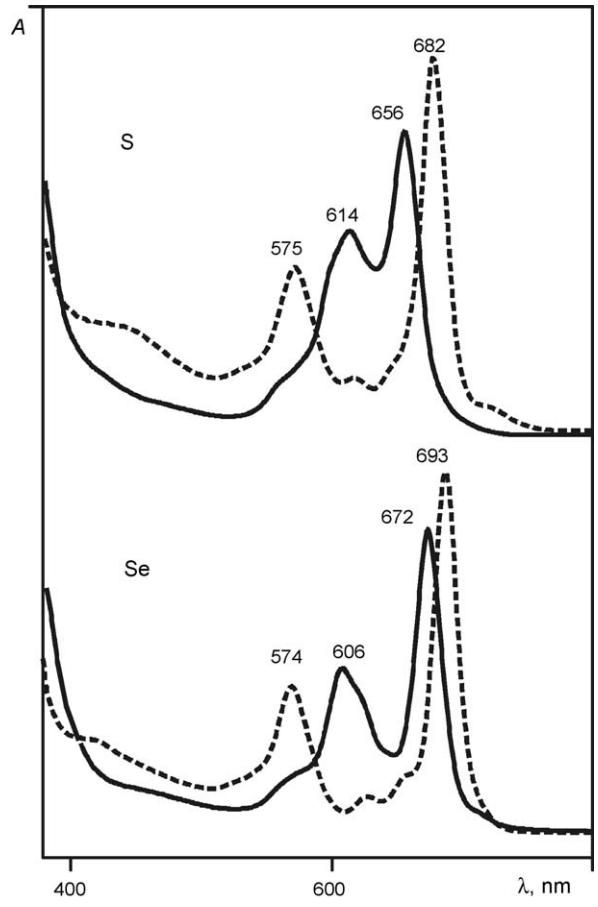

Fig. 18. UV/vis spectra in CH_2Cl_2 of [Ph_6SPzH_2] and [Ph_6SePzH_2] (dashed lines) and [Ph_6SPzZn] and [$Ph_6SePzMg$] (solid lines).

(Table 11). This latter example very clearly illustrates that substitution of two carbon atoms in an annulated thiophene ring by two N atoms as in 1,2,5-thiadiazole means to go from a π-excessive to π-deficient heterocyclic ring, a fact which stabilizes the HOMO by 750 cm^{-1} in respect to LUMO. Although sequential substitution of benzene moieties by thiadiazole rings results in an increasing hypsochromic shift of the Q band maximum, this effect is not strictly additive. Thus, introduction of one, two, three and four thiadiazole rings instead of benzene moieties in octaamyloxyphthalocyanine, [(AmO)$_8$$PcH_2$] (**19**), shifts the position of the Q band maximum from 762 to 766, 735, 721, 715 and 653 nm in [SA_3PzH_2] (**15a**), [$S_2A_2PzH_2$] (**17a**), [$SASAPzH_2$] (**16a**), [S_3APzH_2] (**18a**) and [$TTDPzH_2$] (**5**), respectively, i.e. by 50, 600, 870, 980 and 2400 cm^{-1} in the order given. It should be noted that the spectroscopic properties of the model compounds having methoxy groups instead of amyloxy groups have been calculated by using TDDFT and ZINDO methods [32]. The latter approach provides better agreement of the calculated spectroscopic parameters with experimental UV/vis spectra of amyloxy substituted species.

The splitting of the Q_x and Q_y bands observed for [$TTDPzH_2$] in chlorobenzene (653 and 641 nm, 290 cm^{-1}) is much smaller (Fig. 17 and Table 8) than for [PcH_2] (695 and 659 nm, 710 cm^{-1}) and for [(Pyz)$_4$$PzH_2$] (660 and 625 nm, 850 cm^{-1}) in a similar non-basic solvent. This small splitting observed in

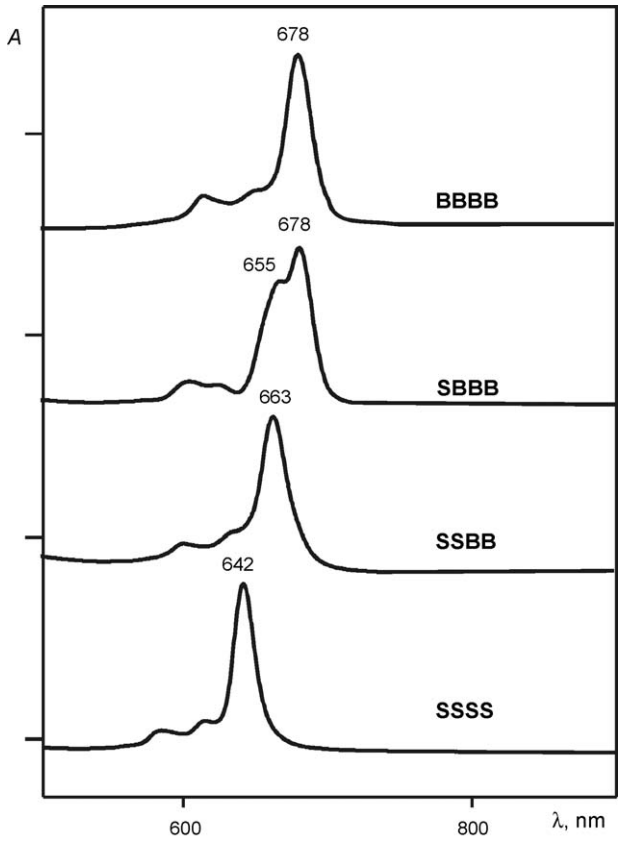

Fig. 19. The Q-band region of the UV/vis spectra in pyridine of Mg^{II}-porphyrazines: symmetrical [TTDPzMg(H_2O)] (SSSS) and [(^{t}Bu)$_4$PcH_2] (BBBB), and low-symmetry [SB_3PzMg] (**21b**) (SBBB) and [S_2B_2PzMg(H_2O)] (**22b**) (SSBB).

solution is not in agreement with the results of quantum chemical calculations [32], which predict a considerable splitting of the Q_x and Q_y bands for [TTDPzH_2] both by the TDDFT method (605 and 570 nm, 1015 cm^{-1}) and ZINDO method (717 and 672 nm, 930 cm^{-1}). Evidently, the energy gap between the LUMO b_{2_g} and b_{3_g} (see Figs. 14 and 15) is strongly overestimated in the calculations as compared to the real situation in solution. This might be indicative of the occurrence of specific intermolecular interactions existing even in the neutral solvents, a situation which was not taken into account in the calculation of the spectroscopic properties of the isolated molecule in the gas phase [32].

4.1.2. Basic solvents

The basic solvents (pyridine, DMF, DMSO) have only moderate solvatochromic effect on the peak position of the Soret- and Q bands in the UV/vis spectra of the metal complexes [TTDPzM] and [TSeDPzM] (M = Mg^{II}(H_2O), Mn^{II}, Co^{II}, Ni^{II}, Cu^{II}, Zn^{II}) [14–17] and [TTDPzMX] (M = Al^{III}, Ga^{III}, In^{III}) [23]. In the case of the free-bases, a peculiar aspect is that the spectra of [TTDPzH_2] and [TSeDPzH_2] in pyridine are similar to those of the related metal complexes since they show an unsplit Q band (see Fig. 20 for comparison of the spectra of [TTDPzH_2] (B) and its Mg^{II} (A) and Ni^{II} (F) complexes), whilst Q band splitting is observed in neutral and acidic solvents (Fig. 20C–E) [14,16,22]. This behavior is due to the combined effect of σ-acceptor and π-deficient properties of the thia/selenodiazole fragments, leading to a high acidity of the central NH groups with implied easy deprotonation and formation of the corresponding symmetrical dianions $[TTDPz]^{2-}$ and $[TSeDPz]^{2-}$ as pyridinium salts. A similar spectroscopic effect can be observed upon addition of a strong base, i.e. tetrabutylammonium hydroxide, to a solution of [TTDPzH_2] in neutral solvents such as CH_2Cl_2 [21,22]. For unsubstituted free-base phthalocyanine and porphyrazine, the deprotonation process can be seen only upon heating or UV-irradiation of the pyridine solutions [76].

Formation of the deprotonated macrocycles as pyridinium salts immediately upon dissolution in pyridine is a clear indication of the high acidity character of the pyrrolic NH groups in porphyrazines. So, whereas no deprotonation is observed for unsubstituted [PzH_2] nor for [PcH_2], porphyrazines with strongly electron-withdrawing substituents (β-halogen, β-sulfophenyl, β-4-methylpyridiniumyl) or annulated electron-deficient heterocycles (tetra(pyrido)-, tetra(pyrazino)porphyrazines) easily form such salts in pyridine and other basic solvents (see Ref. [61] and references therein).

Theoretical investigation of the gas phase acidity of porphyrazines [61] has shown that [TTDPzH_2] has the highest acidity among porphyrazines with different type of tetraannulation. The gas phase acidity decreases in the sequence [TTDPzH_2] > [(Pyz)$_4$PzH_2] > [(^{2,3}Py)$_4$PzH_2] > [PcH_2] > [PzH_2] along with the increase of the deprotonation enthalpy values (304.6, 316.1, 324.8, 331.9, 335.2 kcal/mol, in the sequence given). The experimental value of the acidity constants in DMSO solution pK_{a1} = 1.75 and pK_{a2} = 1.98 have been determined for [TTDPzH_2] by spectrophotometric titration [43,77]. These values of acidity constants are more than 10 orders of magnitude higher than those found for [PzH_2] (pK_{a1} = 12.36 and pK_{a2} = 13.43 in the same solvent [78]).

No formation of the pyridinium salt is observed in pyridine solution for porphyrazines **15a**, **20a**, **21a** with one annulated thia/selenodiazole ring [20,21,24]. If two thiadiazole rings are present as in [S_2A_2PzH_2] (**17a**) and [SASAPzH_2] (**16a**), heating is required for their deprotonation in pyridine. The porphyrazine with three thiadiazole rings [S_3APzH_2] (**18a**) is deprotonated upon dissolution in pyridine just like [TTDPzH_2] [21]. Such behavior is in keeping with the pK_{a1} values determined in DMSO [43,77]. The acidity gradually increases along with annulation of additional thiadiazole rings in the order: [(AmO)$_8$PcH_2] < [SA_3PzH_2] < [S_2A_2PzH_2] < [S_3APzH_2] < [TTDPzH_2] (pK_{a1} = 13.17, 8.80, 8.31, 5.82, 1.75) [43,77] in perfect line with expectation.

4.1.3. Acidic solvents and basic properties

The presence in the molecular framework of thia/selenodiazoloporphyrazines of several basic centers – four *meso*-N atoms (N_{meso}) bridging the pyrrole units, eight N atoms of thia/selenodiazole rings (N_{het}) and in the free-bases two internal pyrrolenine nitrogens (N_{pyr}) – endows these macrocycles with relatively high solubility in acidic media such as HCOOH, CF_3COOH, H_2SO_4, due to specific solvation and acid–base interaction processes. Since all basic centers belong to

Table 11
UV/vis solution spectra of low-symmetry porphyrazines with annulated thia/selenodiazole rings and some related porphyrazines

Porphyrazine	Solvent	λ_{max} (nm) (log ε)[b]				Ref.
$[A_4PzH_2]\equiv[(AmO)_8PcH_2]$ (**19**)	Toluene	329 (4.67)		739 (5.01)	762 (5.09)	[21]
$[SA_3PzH_2]$ (**15a**)	CH_2Cl_2	329 (4.96)		730 (5.02)	766 (5.21)	[21]
$[SeA_3PzH_2]$ (**20a**)	CH_2Cl_2	334 (5.11)		735 (4.90)	785 (5.19)	[20]
$[S_2A_2PzH_2]$ (**17a**)	CH_2Cl_2	336 (4.81)		700sh	735 (4.98)	[21]
$[SASAPzH_2]$ (**16a**)	CH_2Cl_2	333 (4.80)		660sh	721 (4.81)	[21]
$[S_3APzH_2]$ (**18a**)	CH_2Cl_2	335 (4.83)		698sh	715 (4.80)	[21]
$[B_4PzH_2]\equiv[(^tBu)_4PcH_2]$	Toluene	345 (4.84)		662 (5.18)	699 (5.26)	[75]
$[(^{3,4}Th)B_3PzH_2]$	$CHCl_3$	337 (5.08)	648 (5.02)	692 (4.96)	727 (5.25)	[10]
$[SB_3PzH_2]$ (**21a**)		353(*0.39*),		657(*0.59*),	693(*1.00*)	[24]
$[SB_3PzMg]$ (**21b**)	CH_2Cl_2	358(*0.73*)		611(*0.20*)	682(*1.00*)	[24]
$[S_2B_2PzMg]$ (**22b**)	CH_2Cl_2	353(*1.00*)		605(*0.25*)	667(*1.00*)	[24]
$[Ph_8PzH_2]$	$CHCl_3$	370 (4.63)		595 (4.32)	663 (4.48)	[74]
$[Ph_6SPzH_2]$ (**23a**)	CH_2Cl_2	358 (4.45)		575 (4.28)	682 (4.70)	[46]
$[Ph_6SePzH_2]$ (**24a**)		361 (4.55)		574 (4.28)	693 (4.65)	[46]
$[Ph_6BzPzH_2]$				588	691	[46]
$[Ph_6SPzZn]$ (**23c**)				614	656	[46]
$[Ph_6SePzZn]$ (**24d**)				604	670	[46]
$[Ph_6SePzMg]$ (**24b**)	CH_2Cl_2	364		606	672	[46]
$[Ph_6SePzCu]$ (**24c**)	CH_2Cl_2			608	668	[46]
$[Ar_6SePzH_2]$[a] (**25a**)	CH_2Cl_2	342		579	710	[31]
$[Ar_6SePzMg]$[a] (**25b**)	CH_2Cl_2	362		617	689	[31]
$[Ar_6SePzCu]$[a] (**25c**)	CH_2Cl_2	342, 456	550	616	685	[31]
$[Pr_8PzH_2]$		346		558	627	[31]
$[Pr_6\{PyzMe_2\}PzH_2]$	CH_2Cl_2	340 (4.74)		565 (4.57)	634 (4.71)	[29]
$[Pr_6SePzH_2]$ (**26a**)	CH_2Cl_2	346 (4.81)		552 (4.60)	653 (4.87)	[29]
$[Pr_6SePzMg]$ (**26b**)	CH_2Cl_2	346 (4.52)		599 (4.19)	650 (4.12)	[29]
$[Pr_6SePzMn(Cl)]$ (**26e**)	CH_2Cl_2	361		618	679	[30]
$[Pr_6SePzNi]$ (**26c**)	CH_2Cl_2	332 (4.51) 346 (4.51)		578 (4.36)	634 (4.37)	[31]
$[Pr_6SePzCu]$ (**26d**)	CH_2Cl_2	339 (4.58) 354 (4.63)	581 (4.41)	593 (4.42)	636 (4.50)	[31]

[a] Ar: 3,4,5-trimethoxyphenyl.
[b] Relative intensity (D/D_{max}) is shown in italics.

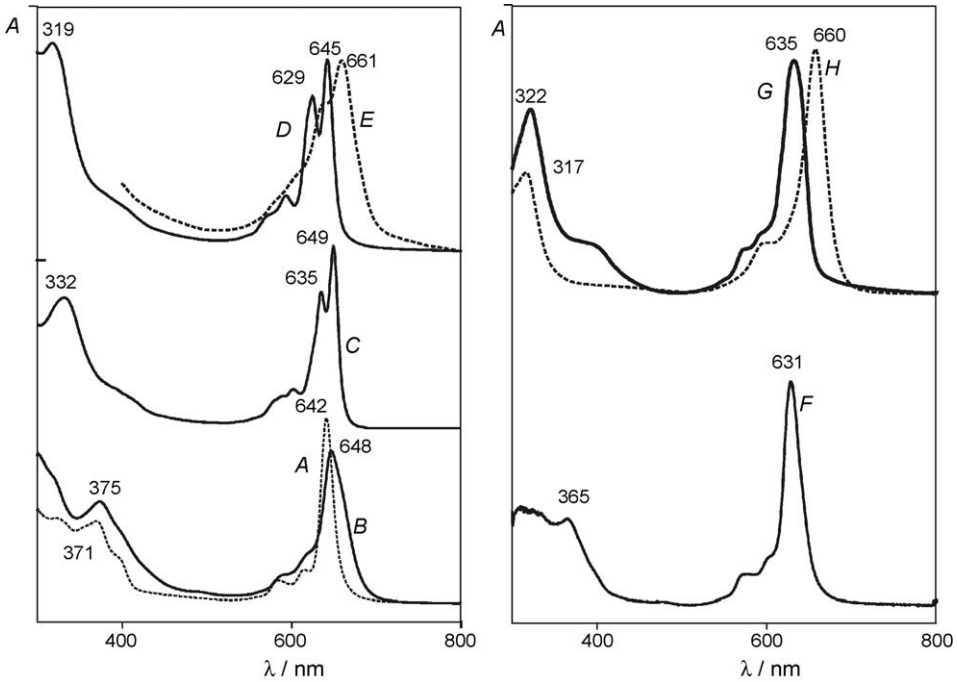

Fig. 20. UV/vis spectra of $[TTDPzMg(H_2O)]$ (*A*), $[TTDPzH_2]$ (B–E) and [TTDPzNi] (F–H) in pyridine (A, B and F). CH_2Cl_2 (C), CF_3COOH (D and G) and in H_2SO_4 (E and H). Spectrum B shows the pyridinium salt $[TTDPz]^{2-}(H^+Py)_2$. Spectra of $[TTDPzMg(H_2O)]$ in CF_3COOH and in H_2SO_4 are identical to the spectra D and E.

the conjugated π-chromophore, a strong solvatochromic effect determined by the acidity of the media is a characteristic feature of diazoloporphyrazines. Stable solutions are obtained in CF_3COOH for all investigated free-bases and related metal complexes, exception made for the Mg^{II} species, due to demetalation. Free-bases undergo hydroprotolytic destruction in aqueous concentrated H_2SO_4 but are more stable in non-aqueous H_2SO_4. [TTDPzH$_2$] is by 10 times less stable than the Se-analogue, the rate constants of their destruction in 96.6% aqueous H_2SO_4 at 25 °C being 910×10^5 and 56×10^5 s^{-1}, respectively [22]). Complexes with Zn^{II}, Cu^{II}, Ni^{II}, Co^{II}, Mn^{II}, Al^{III} and Ga^{III} are stable in concentrated aqueous H_2SO_4 solutions at ambient temperatures, but slow demetalation is observed for In^{III} and instantaneous for Mg^{II} complexes. The order of kinetic stability has been determined for the group III metals complexes [TTDPzMX]: $Al^{III} > Ga^{III} > In^{III}$ (the corresponding rate constants of dissociation $k_{obs} \times 10^5$ are 3.88, 18.7, 181 s^{-1} in 16.9 M H_2SO_4 at 51 °C [23]).

For [TTDPzH$_2$] and [TSeDPzH$_2$] and their metal complexes only a slight hypsochromic shift of the Q band (up to 200 cm^{-1}) or its broadening is observed even in strong carboxylic acids such as HCOOH and CF_3COOH (Hammet acidity function H_0 is −2.22 [79] and −3.03 [80], respectively). The Soret band envelope becomes more sharp. These spectroscopic changes suggest acid solvation or partial protonation occurring at the N atoms of annulated thia/selenodiazole rings. For the unmetalated macrocycles, the splitting of the Q band becomes more well-defined, this demonstrating that no protonation of internal pyrrolenine N atoms is taking place in these media. In H_2SO_4 for [TTDPzH$_2$] and [TSeDPzH$_2$] and their metal complexes, a bathochromic shift of the Q band is observed (15–30 nm, 500–800 cm^{-1}) which is indicative of protonation of one of the *meso*-N atoms.

The basicity constants pK_{a1} for protonation of the first *meso*-N atom have been determined in CF_3COOH-H_2SO_4 mixtures for [TTDPzH$_2$] (pK_{a1} = −4.06), [TTDPzZn] (−6.28), [TTDPzCu] (≈−8 to −9) and [TTDPzNi] (−5.81) [12]. The basicity of the *meso*-N atom in [TTDPzH$_2$] and its complexes is several orders of magnitude lower than for [PzH$_2$] (pK_{a1} = −0.15 [81]) or [PcH$_2$] and their corresponding metal complexes [82]. This fact reflects the strong electron acceptor effect of four thiadiazole rings resulting in a drastic decrease of the basic properties. The pK_{a1} for the Zn^{II} and Cu^{II} complexes are lower than for the Ni^{II} complex and the related free-base [TTDPzH$_2$]. This is unusual, since for the series of [PzM] and [PcM] complexes a different order of basicity is observed, Zn > Cu > 2H > Ni [82]. This fact is a clear indication that in the case of [TTDPzZn] and [TTDPzCu] protonation of *meso*-N atoms follows protonation of the thiadiazole rings.

Unlike [TTDPzH$_2$] and [TTDPzM] which only give *meso*-monoprotonated forms in H_2SO_4 solution, for monoannulated porphyrazine [SB_3PzH_2] (**21a**, Table 2) and its Cu^{II} complex [SB_3PzCu] (**21c**) in CH_3COOH–H_2SO_4 media it was possible to observe [25] a stepwise acid–base interaction with all four *meso*-N atoms. It results in an increasing bathochromic shift of the Q band maxima from 690 nm for [SB_3PzH_2] and 683 nm for [SB_3PzCu] in a neutral solvent to 820 and 785 nm in 93–100% H_2SO_4, respectively (Δλ(Q) = 130 and 102 nm (2290 and 2080 cm^{-1})) (see Fig. 21 for the spectra of [SB_3PzH_2]). It was shown that along with protonation of the second *meso*-N atom one of the thiadiazole N atoms is involved in acid–base interaction. Whilst annulation of the thiadiazole ring due to its electron-acceptor properties reduces the basicity of *meso*-N atoms (pK_{ai} = −1.10, −2.75, −5.83, −8.44 for [SB_3PzH_2] and −0.90, −1.40, −4.86, −7.80 for [SB_3PzCu] [25]) as compared with tetra(*tert*-butyl)phthalocyanines (pK_{ai} = +0.86, −1.58, −4.60, −7.05 for [$^tBu_4PcH_2$] and +2.10, −0.33, −3.03, −6.23 for [$^tBu_4PcCu$] [83]), the basicity of N atoms of thiadiazole ring itself (pK_a(N_{het}) = −4.25 for [SB_3PzH_2] and −2.20 for [SB_3PzCu] [25]) is increased as compared to non-annulated 1,2,5-thiadiazole (pK_a = −4.90 [63]).

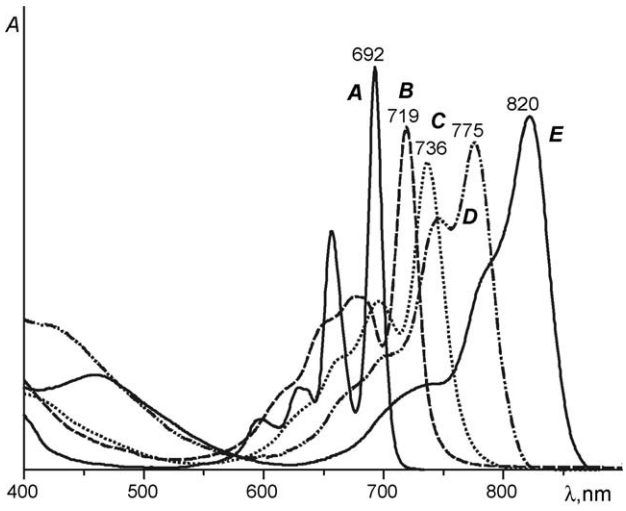

Fig. 21. UV/vis spectra of [SB_3PzH_2] (**21a**) in CH_2Cl_2 (A) and its acid forms in CH_3COOH containing 4.9% (B), 29.7% (C), 58% (D) and 93% (E) H_2SO_4.

The effect of replacing two β-phenyl groups in β-octaphenylporphyrazine, [Ph_8PzH_2], and its Zn^{II} complex, [Ph_8PzZn], by one thiadiazole, selenodiazole or benzene ring has been studied in CH_2Cl_2–CF_3COOH solutions [43,46] and the stability constants pK_{s1} of the first acid form were determined. Annulation of the aromatic ring decreases the basicity of *meso*-nitrogen atoms and this effect is increased in the order benzene < selenodiazole < thiadiazole (Table 12).

Sequential substitution of benzene moieties in octaamyloxyphthalocyanine [$(AmO)_8PcH_2$] by thiadiazole rings has a marked effect on the basicity macrocycle and its spectroscopic behavior in acidic media [77,84]. Whilst all four *meso*-N atoms in [$(AmO)_8PcH_2$] (≡[A_4PzH_2] (**19**)) and [SA_3PzH_2] (**15a**) are protonated in going from a neutral solvent to 100%

Table 12
Influence of aromatic annulation in β-phenyl substituted porphyrazines on the stability constant of the first acid form in CH_2Cl_2–CF_3COOH at 298 K [46]

Free-base	pK_{s1}	Zn^{II} complex	pK_{s1}
[Ph_8PzH_2]	1.43	[Ph_8PzZn]	2.63
[Ph_6BzPzH_2]	1.02	[$Ph_6BzPzZn$]	2.42
[Ph_6SPzH_2]	0.55	[Ph_6SPzZn]	2.27
[Ph_6SePzH_2]	0.65	[$Ph_6SePzZn$]	2.44

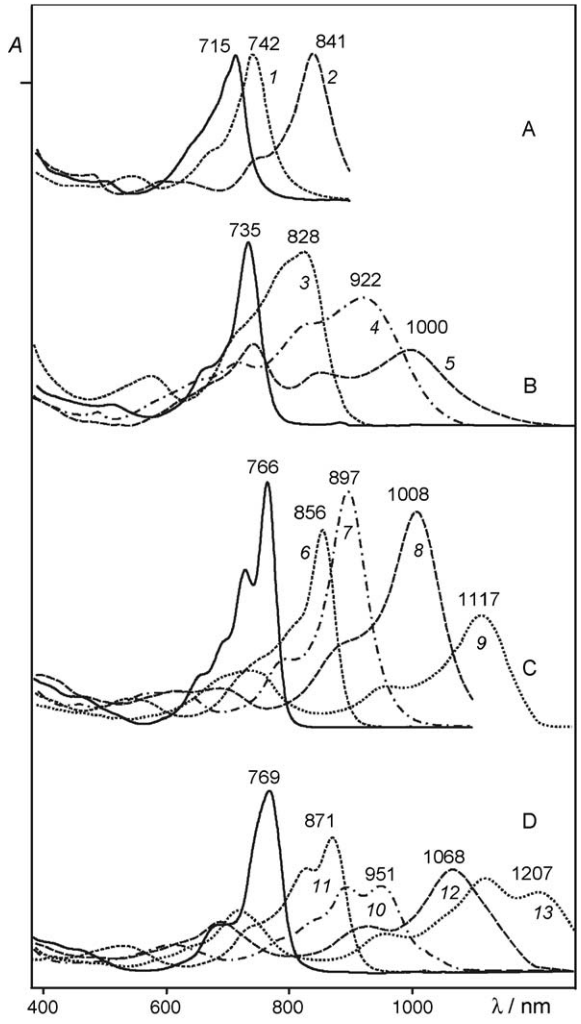

Fig. 22. UV/vis spectra of $[S_3APzH_2]$ (**18a**) (A), $[S_2A_2PzH_2]$ (**17a**) (B), $[SA_3PzH_2]$ (**15a**) (C) and $[A_4PzH_2]$ (**19**) (D) in CH_2Cl_2 (solid lines) and their acid forms in CH_2Cl_2 containing 0.5% (10), 5% (6 and 11), 100% (7) HCOOH, in CF_3COOH (1 and 3), in CF_3COOH containing 1% H_2SO_4 (4 and 12), in CH_3COOH containing 35% H_2SO_4 (8) and in 96% H_2SO_4 (2, 5, 9 and 13) (figure modified from Ref. [21]).

H_2SO_4, only three of them are protonated for $[S_2A_2PzH_2]$ (**17a**) and two for $[S_3APzH_2]$ (**18a**) under identical conditions (Fig. 22).

The influence of the number of annulated rings on the basicity of *meso*-N atoms in this series of free-bases as well as their Zn^{II} complexes can be evaluated from the stability constants pK_{s1} of the first acid form obtained in CH_2Cl_2–CF_3COOH medium [43,77,84]. For the free-bases, the pK_{s1} decrease in the order $[SA_3PzH_2]$ (3.89) > $[A_4PzH_2]$ (3.52) > $[S_2A_2PzH_2]$ (2.27) > $[SASAPzH_2]$ (2.19) > $[S_3APzH_2]$ (0.83) and for the Zn^{II} complexes $[SA_3PzZn]$ (4.80) > $[A_4PzZn]$ (3.58) > $[S_2A_2PzZn]$ (3.51) > $[S_3APzZn]$ (2.81). This sequence demonstrates that the larger the number of thiadiazole rings present, the lower the basicity of the *meso*-N atoms. In the phthalocyanines $[A_4PzH_2]$ and $[A_4PzZn]$ the *meso*-N atoms are less basic than in the species $[SA_3PzH_2]$ and $[SA_3PzZn]$ having one annulated thiadiazole ring. This is due to the strong polarization of the π-electron system in the two latter monoannulated species which shifts π-electrons from benzene ring in the direction of the thiadiazole rings and results in an increase of the electron density on *meso*-N atoms overriding the σ-acceptor effect of the thiadiazole rings. Interestingly, the basicity of the *trans*-annulated porphyrazine $[SASAPzH_2]$, in which all *meso*-N atoms connect isoindole and thiadiazolepyrrolenine units, is lower than that of the *cis*-isomer $[S_2A_2PzH_2]$ in which two *meso*-N atoms are located between two more electron rich isoindole and isoindolenine fragments.

4.2. Vibrational spectra

The IR spectra of $[TTDPzH_2]$, its Se-analogue $[TSeDPzH_2]$ and their metal complexes were examined and discussed [14–17]. The main IR modes were assigned on the basis of the comparison with the data available for 1,2,5-thia- and 1,2,5-selenodiazoles [85,86] and other tetrapyrrolic macrocycles [87]. Fig. 23 reports the IR spectra of $[TTDPzH_2]$, $[TSeDPzH_2]$ and their Ni^{II} complexes as representative species for the metal derivatives.

For $[TTDPzH_2]$ and $[TSeDPzH_2]$ the NH stretching vibrations, ν(NH), appear at 3290 and 3280 cm^{-1} and the NH out-of-plane deformations γ(NH) at 753 cm^{-1}. For $[TTDPzH_2]$, the assignments for both modes was made [14] by deuteration and for $[TTDPzD_2]$ ν(ND) and γ(ND) were found at 2465 and 585 cm^{-1}, respectively. The in-plane NH deformations, δ(NH), are strongly coupled with the vibrations of the pyrrole ring and their assignment is not straightforward. In the region of the in-plane deformation modes (1000–1600 cm^{-1}), the IR spectra of the free-bases are different from the spectra of the corresponding metal complexes because of the presence in the former species of weak-to-medium bands at 1565 and 1535 cm^{-1}, strong bands at 1215 and 1210 cm^{-1} and medium-strong bands at 1014 and 1030 cm^{-1}, for $[TTDPzH_2]$ and $[TSeDPzH_2]$, respectively (Fig. 23). Initially, the δ(NH) mode in $[TTDPzH_2]$ has been associated [14] with the band at 1565 cm^{-1} on the basis of the assignment made for the 1539 cm^{-1} band in the case of $[PcH_2]$ [88]. However, in the case of porphyrins [87] and unsubstituted porphyrazine [89,90] the deuteration experiments and calculations of the potential energy distribution have shown that the local δ(NH) mode highly contributes to the band in the 1210–1260 cm^{-1} region. The recent theoretical study [91] reinterpreted the assignment of the in-plane NH vibrations in the IR spectra of $[PcH_2]$ and suggested that the δ(NH) mode corresponds to the 1250 cm^{-1} band. Taking these results into account, it can be concluded that also for $[TTDPzH_2]$ and $[TSeDPzH_2]$ δ(NH) vibration have the highest contribution in the band near 1210–1215 cm^{-1}.

The vibrations of the central porphyrazine core are strongly coupled with those of annulated heterocycles. As a result, the TTDPz and TSeDPz macrocycles have a unique IR spectroscopic pattern which is quite different from those of their phthalocyanine and other porphyrazine analogues. Some pertinent assignments were suggested [17]. The stretching vibrations of the *meso*-N atom bridge, $\nu(CN_{meso})$, give weak-medium IR bands in the 1500–1550 cm^{-1} region. The skeletal vibrations of pyrrole rings, ν(Pyr), are strongly mixed with the ν(C=N)

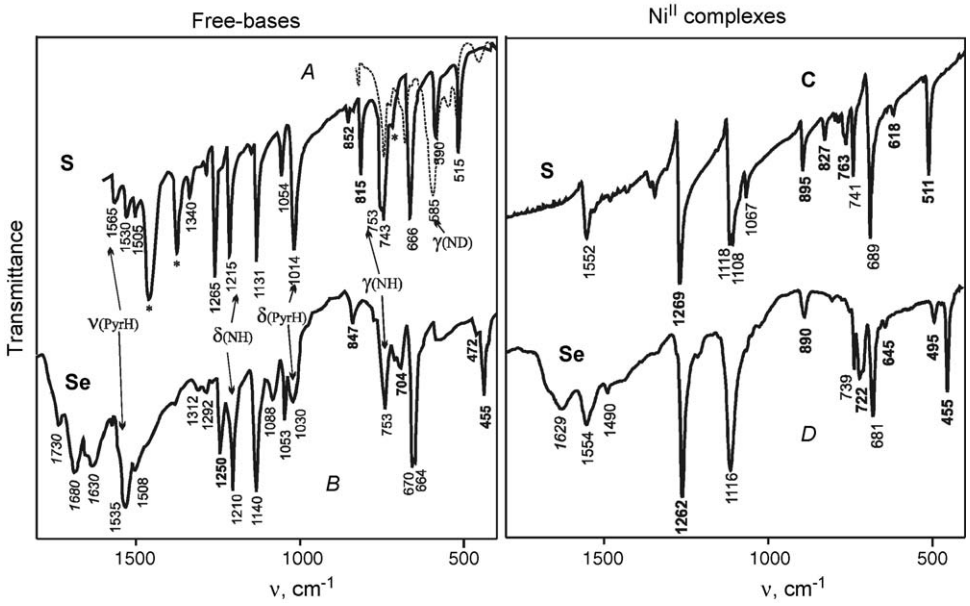

Fig. 23. IR spectra of [TTDPzH$_2$]: (A, the dashed line is for deuterated material), [TSeDPzH$_2$] (B) and their Ni^{II} complexes (C and D) in nujol (A) and KBr (B–D). Position of peaks associated with annulated 1,2,5-thia/selenodiazole rings are given in bold-type, and those in italics are related to solvent molecules.

vibrations of the annulated thia/selenodiazole rings and give the most intense IR band at 1240–1270 cm^{-1}. The in-plane deformations of the pyrrolenine rings, δ(Pyr), give a strong IR band at 1080–1140 cm^{-1} and a weak-medium band at 1050–1060 cm^{-1}. For free-bases, an additional strong band of the in-plane pyrrole deformations δ(PyrH) is present at 1010–1030 cm^{-1}. The out-of-plane deformations of pyrrole rings γ(Pyr) appear at 660–670 cm^{-1} for the free-bases and are shifted to higher energy to 680–690 cm^{-1} for the metal complexes.

Some local modes of the annulated heterocyclic rings can be also assigned by comparison of the IR spectra of thia/selenodiazoloporphrazines [14–17] with those of the 1,2,5-thia- and 1,2,5-selenodiazoles [85,86]. Thus, the stretching vibrations of the SN and SeN bonds which are strong in 1,2,5-thia- and 1,2,5-selenodiazoles (ν(SN) 806 and 780 cm^{-1} and ν(SeN) at 728 and 589 cm^{-1} [85,86]) give bands of weak-medium intensity for TTDPz (ν(SN) at 810–830 and 760–770 cm^{-1}) and TSeDPz macrocycles (ν(SeN) at 700–725 and 640–650 cm^{-1}). The strong in-plane deformations of the annulated heterocycle appear near 850 cm^{-1} in the free-bases and near 890 cm^{-1} in metal complexes, whilst they are observed at 895 and 880 cm^{-1} in 1,2,5-thia- and 1,2,5-selenodiazoles [85,86]. The out-of-plane deformations of the heterocycles give weak bands at 615–625 and 480–495 cm^{-1} for S- and Se-porphyrazines, respectively. The ring torsion vibrations of the annulated heterocycles appear as strong bands at 515–510 and 450–465 cm^{-1} for TTDPz and TSeDPz, respectively. Being only slightly shifted from their position in 1,2,5-thia- and 1,2,5-selenodiazoles (520 and 438 cm^{-1}), they provide the most clear indication of the presence of the annulated thia- or selenodiazole rings in the porphyrazine macrocycle and their intensity correlates with the number of heterocycles present in each species [21].

The FT-Raman spectra were reported [17] for the Ni^{II} complexes [TTDPzNi] and [TSeDPzNi] (Fig. 24). Although excitation wavelength λ_{ex} = 1064 nm is far from the position of the Q band maxima, the vibrations of the annulated heterocycles have low intensity and only the vibrations of the bonds forming the central porphyrazine π-chromophore are strongly

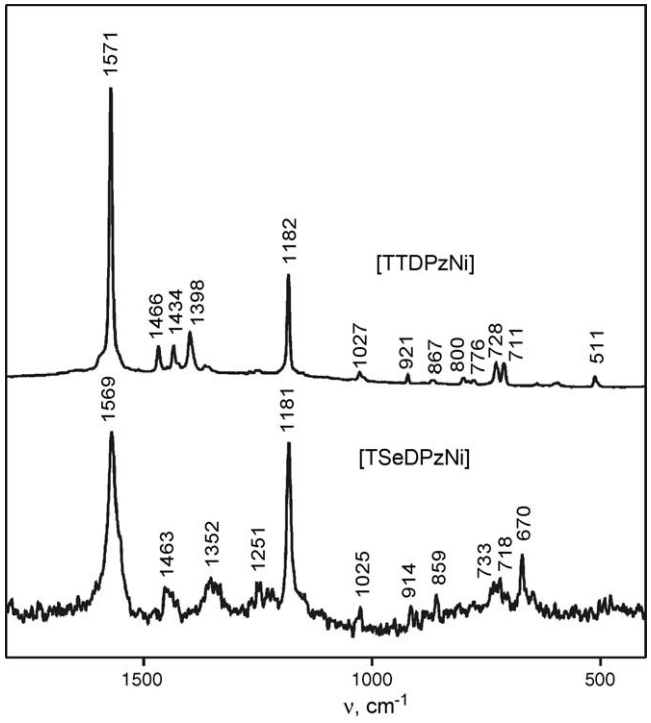

Fig. 24. FT-Raman spectra of [TTDPzNi] and [TSeDPzNi] obtained at λ_{ex} = 1064 nm (redrawn from Ref. [17]).

enhanced. Whilst the stretching vibrations of the *meso*-N atom bridged moiety, $\nu(CN_{meso})$, appear as weak-medium bands at 1500–1550 cm^{-1} in the IR spectrum, they give the strongest band near 1570 cm^{-1} in the FT-Raman spectrum. Another strong RR band which is observed at ca. 1180 cm^{-1} belongs to pyrrole in-plane deformations δ(Pyr). Noteworthy, these strong bands show no dependence from the chalcogen atom (S or Se) in the annulated ring.

4.3. Optical limiting

As is well known, highly π-conjugated systems like phthalocyanines, porphyrins and porphyrazines are extensively explored for their non-linear optical behavior [92,93]. Porphyrazines combining thiadiazole and benzene annulation were investigated with regard to their third order non-linear optical properties (optical limiting) [21] and theoretically as potential two-photon absorption materials [32]. Symmetrical species, $[TTDPzH_2]$ and $[(AmO)_8PcH_2]$, and related low-symmetry porphyrazines, $[SA_3PzH_2]$ (**15a**) and $[S_2A_2PzH_2]$ (**17a**), display an optical limiting behavior in respect to the intense nanosecond pulses of the 2nd harmonics of the Nd:YAG laser (532 nm). All species exhibit an optical limiting effect according to the reverse saturable absorption mechanism due to sequential two-photon absorption. It was shown that in the series $[(AmO)_8PcH_2]$ (**19**), $[SA_3PzH_2]$ (**15a**), $[S_2A_2PzH_2]$ (**17a**), $[TTDPzH_2]$ (**5**) the optical limiting performance is decreased along with increasing the number of annulated thiadiazole rings. This can be due to the variation of the intersystem crossing efficiency ($S_1 \rightarrow T_0$) and/or the ($T_0 \rightarrow T_1$) absorption cross-section.

In order to evaluate other non-linear optical applications, two photon absorption (TPA) spectra have been calculated for $[TTDPzH_2]$, $[(MeO)_8PcH_2]$ and four low-symmetry porphyrazines containing fused thiadiazole and dimethoxybenzene moieties [32]. All of these species were shown to have the main TPA maximum λ^2_{max} in the 750–860 nm region and for some of them an additional maximum of lower intensity is expected at 1050–1150 nm. All species, and especially those having electron-donating benzene moieties in *trans*-position, have a very high value of TPA cross-section ranging from 1018 GM at 861 nm for $[TTDPzH_2]$ to 1103 GM at 800 nm for *cis*-2:2 and to 4447 GM at 790 nm for the *trans*-2:2 species. These values are reported to be some orders of magnitude higher than those of commercial organic dyes [32]. Thus, these compounds are promising materials for a number of applications requiring strong TPA absorption, i.e. ultra-high-density optical data storage, biological imaging, three-dimensional microfabrication [32].

5. Axial coordination and electrochemical properties

The electron-withdrawing properties of the TTDPz macrocycle determine coordinative unsaturation for the Mn^{II}, Fe^{II}, Co^{II}, and even for Ni^{II} derivatives. The Mn^{II} and Fe^{II} complexes form stable isomorphous bisadducts with DMSO of formulae $[TTDPzMn(DMSO)_2]$ and $[TTDPzFe(DMSO)_2]$. These are directly obtained by reaction of the free-base ligand $[TTDPzH_2]$ with M^{II} salts in hot DMSO (200 °C) [15]. DMSO is strongly ligated at the axial positions of the two metal centers and requires drastic conditions for its elimination. Noticeably, a Pc analogue is known for Fe^{II}-phthalocyanine, $[PcFe(DMSO)_2]$, but the corresponding Mn^{II} complex has not so far been reported. The Fe^{II} species $[TTDPzFe(DMSO)_2]$ is a d^6 low-spin complex as proved by magnetic and Mössbauer data. The room temperature μ_{eff} value of 4.17μ_B for the Mn^{II} bis-adduct is suggestive of an intermediate spin state, but no variable temperature magnetic studies were conducted [15]. It is known that DMSO can ligate to a central metal through either sulfur or oxygen [94]. Detailed examination of the IR spectra of both the present species containing DMSO or DMSO-d_6 unequivocally established that the DMSO molecules are O-ligated, and not S-ligated to the central metal, as was found by X-rays for $[PcFe(DMSO)_2]$ [95] and also for $[PcRu(DMSO)_2]$ [96].

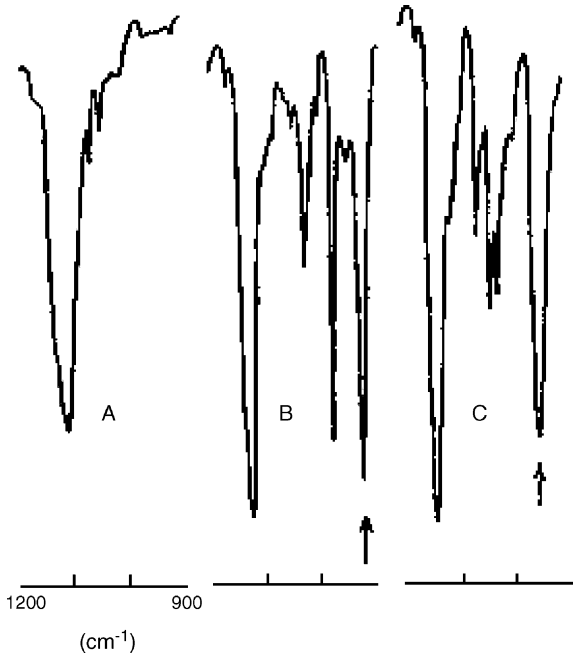

Fig. 25. The 900–1200 cm^{-1} region of the IR spectra of $[TTDPzFe]\cdot 2H_2O$ (A), $[TTDPzFe(DMSO)_2]$ (B), $[TTDPzFe(DMSO\text{-}d_6)_2]$ (C).

Fig. 25 illustrates this point for the Fe^{II} complex. The 1200–900 cm^{-1} is the region where the S–O stretching mode for uncoordinated DMSO is found (ca. 1055 cm^{-1}). Coordination through S should shift the S–O stretching mode to higher frequency, whereas coordination through O should locate the mode at lower frequency values, roughly in the range 950–900 cm^{-1}. Fig. 25 shows that in a region free from other absorptions (1100–900 cm^{-1}, see Fig. 25A for the Fe^{II} bishydrate as reference), an intense absorption, assigned as ν(SO), is found at 918 cm^{-1} for the DMSO adduct (Fig. 25B), shifted to 932 cm^{-1} if DMSO-d_6 is used (Fig. 25C). Analogous information led to the assumption of an O-ligated DMSO also for the complex $[TTDPzMn(DMSO)_2]$ (ν(SO) at 940 cm^{-1} for DMSO and 965 cm^{-1} for DMSO-d_6).

Solid stable bispyridine adducts of the type $[TTDPzM(py)_2]$ are formed not only for M = Mn^{II}, Fe^{II} and Co^{II}, but even for Ni^{II}. This series of bis-adducts, previously mentioned [33] were

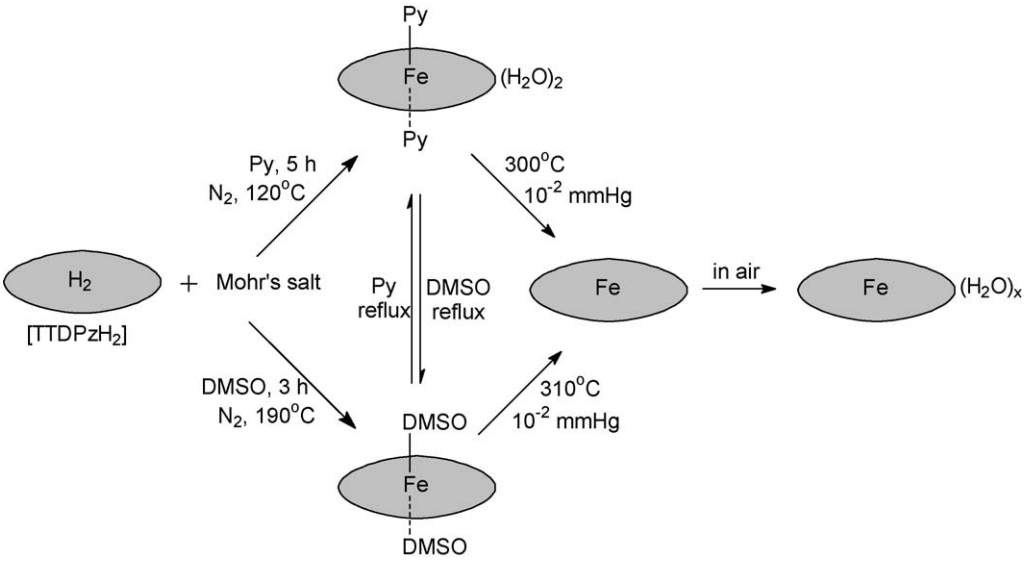

Scheme 8.

prepared by us and have not so far been described in detail. The formation of these adducts points to the strong Lewis acidity of the central metal ion in the species [TTDPzM] (M = Mn^{II}, Fe^{II}, Co^{II}, Ni^{II}). The corresponding phthalocynine complexes also form bispyridine adducts, [PcM(py)$_2$] for M = Mn^{II}, Fe^{II} and Co^{II}, structurally elucidated [97,98], but a similar adduct is not formed by [PcNi], a fact which is probably related to the lower electron deficiency of the Pc macrocycle.

The great stability of the TTDPz macrocycle allows easy interconversion of the different adducts, hydrated and anhydrous species, as it is exemplified in Scheme 8 for the Fe^{II} species.

There appears to be in general a lower tendency of the Se-species [TSeDPzM] (M = Mn^{II}, Co^{II}, Ni^{II}, Zn^{II}) to axial ligation as shown for instance by the fact that no DMSO adducts could be isolated for these species in their preparation in this solvent [17]. Besides, the synthesis of the complexes carried out in pyridine leads to the formation of only monoadducts of formula [TSeDPzM(py)]. This is clearly the effect of a lower electron deficiency in the Se-porphyrazine framework than in the S-containing macrocycles, in keeping with information derived from the UV/vis spectroscopic data illustrated in Section 4.1. On the other hand, the Se-porphyrazines confirm that their behavior is more similar to that of the corresponding phthalocyanine analogues.

Axial coordination is obviously present in the recently reported TTDPz macrocycles containing Al^{III}, Ga^{III} and In^{III} due to the presence of the apical Cl^- (Al^{III}, Ga^{III}) or AcO^- (In^{III}) ions [23]. For the Al^{III} and Ga^{III} complexes, which incorporate only electro-inactive metal centers and hence the uptake of electrons can only occur on the macrocycle (only processes in the cathodic region, 0 to −2.0 V versus SCE are observed) electrochemical studies in solution show the presence of equilibria in pyridine or DMF involving species with axially coordinated solvent.

An example is shown for [TTDPzAlCl] in Fig. 26 which reports the cyclic voltammograms for the first two reduction processes of the compound in DMF before and after the addition of TBACl to the solution. The first one-electron reduction is located at $E_{1/2}$ = −0.10 V in DMF, 0.1 M TBAP and is reversible when the negative potential sweep is reversed at −0.40 V (Fig. 26A). However, this process becomes irreversible and involves a coupled chemical reaction on the reoxidation step if the reversed scan is initiated at −0.80 V (Fig. 26B), a point negative of the

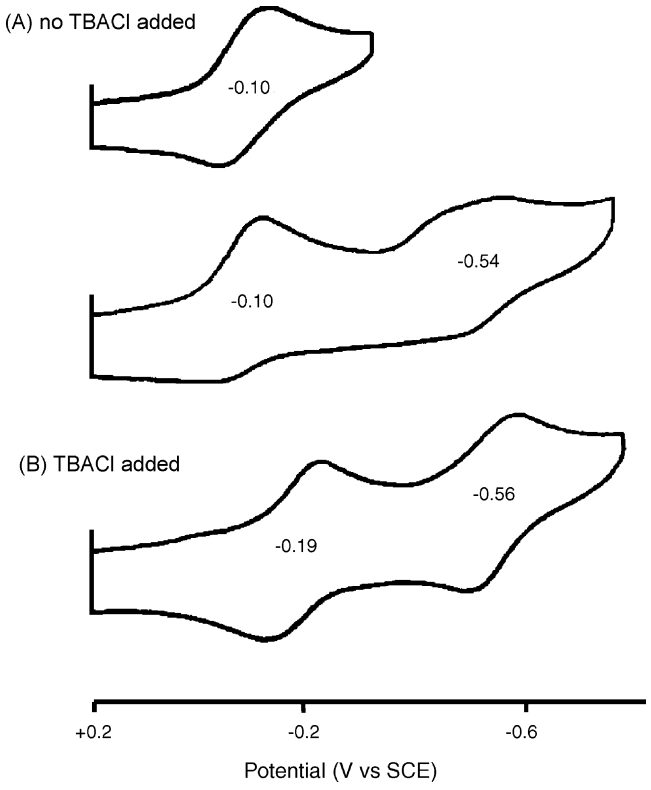

Fig. 26. Cyclic voltammograms of [TTDPzAlCl] in DMF (0.1 M TBAP): (A) before and (B) after addition of excess TBACl to solution. Scan rate = 100 mV/s.

second reduction which is split into two closely spaced processes at $E_p = -0.48$ and -0.58 V for a scan rate of 0.10 V/s.

The type of current–voltage curves for first reduction in Fig. 26 are what would be expected for an equilibrium involving [TTDPzAlCl] and solvated $[TTDPzAl(DMF)_x]^+$, the latter of which should be easier to reduce by virtue of the overall positive charge on the complex. This equilibrium is shown in Eq. (1) and can be shifted to the left by the addition of excess Cl^- to the solution. This is illustrated by the cyclic voltammogram in Fig. 26B:

$$[TTDPzAlCl] + x\text{DMF} = [TTDPzAl(DMF)_x]^+ + Cl^- \quad (1)$$

where $E_{1/2}$ for the first reduction shifts from -0.10 to -0.19 V. The reduction at $E_{1/2} = -0.10$ V is assigned to the DMF solvated form of the Al^{III} complex whilst the process at $E_{1/2} = -0.19$ V is assigned as a reduction of the compound which still maintains the bound Cl^- anion.

An equilibrium of the type shown in Eq. (1) also occurs for [TTDPzAlCl] and [TTDPzAlOH] and for the parallel Ga^{III} species in pyridine [23]. In all cases studied, more complex situations are observed at more negative potentials after the second reduction due to an involvement of the electroreduced species in one or more chemical reactions, some or all of which involve pyridine.

Ill-defined reductions are seen for the In^{III} complex, [TTDPzIn(OAc)], although the first reduction at $E_{1/2} = -0.26$ V seems to be clear. Several additional ill-defined peaks are present on the cathodic or anodic potential scans and these are due to different coordinated forms of the electroreduced species which exist in pyridine.

Table 13 shows that the first one-electron reductions of the [TTDPzMX] complexes are all extremely facile. The process at $E_{1/2} = -0.07$ V for [TTDPzAlCl] and -0.13 V [TTDPzGaCl] in pyridine gives in both cases the π-anion radical $[TTDPzM(py)_x]$ where $x = 1$ or 2. The second reduction of [TTDPzMX] gives the dianion and is also quite facile. Worthy of notice, the measured $E_{1/2} = -0.54$ V for the second reduction of [TTDPzAlCl] in pyridine (or DMF) is virtually identical to the half-wave potential for the first reduction of [PcAlCl] in the same solvent/supporting electrolyte mixture (-0.55 V versus SCE). From these data it can be derived that by substituting the benzene rings in the phthalocyanine macrocycle by the strongly electron-deficient thiadiazole rings the electron uptake and the concomitantly occurring negative charge redistribution within the macrocycle are highly facilitated.

The spectroscopic changes observed during the first two one-electron reduction waves of the Al^{III} complex, [TTDPzAlCl], in pyridine (Fig. 27) indicate full reversibility of the redox processes. Fig. 27A shows the spectroscopic changes which occur during first reduction of [TTDPzAlCl] at a fixed applied potential of -0.34 V versus SCE to give [TTDPzAl] as a final product (coordination of pyridine is neglected). The practically complete disappearance of the intense Q band at 649 nm is accompanied by a shift of the B band from 340 to 362 nm and the appearance of new bands at 433, 536 (sh), 554 and 926 nm. These spectroscopic changes parallel those obtained for the Pc analogue [PcAlCl] [99] and are assigned to the formation of the π-anion radical [TTDPzAl]. Quite similar spectroscopic changes are seen during the first one-electron reduction of the Ga^{III} and In^{III} analogues, [TTDPzGaCl] and [TTDPzIn(OAc)].

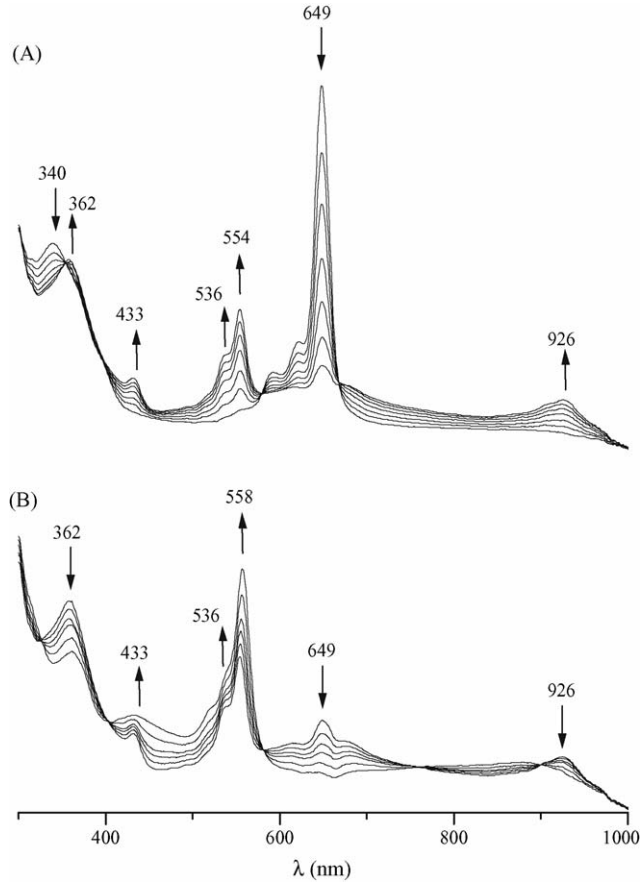

Fig. 27. UV/vis spectroscopic changes in pyridine containing 0.2 M TBAP during controlled-potentials electrolysis of [TTDPzAlCl] at (A) -0.34 V (first reduction, first scan) and (B) -0.70 V (second reduction, first scan).

Electrogeneration of the dianionic Al^{III} species $[TTDPzAl]^-$ at -0.7 to -0.8 V gives spectroscopic changes which mainly consist of a strong intensity increase with minor shifts of the absorption bands assigned to the $\pi^* \rightarrow \pi^*$ transitions at 530–560 nm, accompanied by some shifts and changes of the lower intensity first and second $\pi \rightarrow \pi^*$ transitions. This is illustrated in Fig. 27B which shows the spectroscopic changes which occur during the second reduction of [TTDPzAlCl] to give $[TTDPzAl]^-$. It is known from the literature [100] that the characteristic feature of the second reduction and formation of the π-dianion for metal phthalocyanine complexes with redox

Table 13
Half-wave potentials (V vs. SCE) for first and second reductions of [TTDPzM(X)] and [PcM(X)] [23]

M(X)	[TTDPzM(X)]	[PcM(X)]	Solvent
Al(Cl)	−0.07, −0.54	−0.55, −0.90	py
	−0.10, −0.54	−0.55, −1.00	DMF
Ga(Cl)	−0.13, −0.55	−0.53, −0.84	py
In(X)	−0.26 (X = OAc)	−0.67, −0.94 (X = Cl)	py

inactive central metals is a hypsochromic shift of the $\pi^* \rightarrow \pi^*$ transition band which retains its intensity.

Acknowledgements

The authors are highly indebted to all colleagues, co-workers, and postgraduates and students, co-authors who substantially contributed to the joint study of the thia/selenodiazoloporphyrazines. Special thanks go to Prof. K. Awaga (Japan), Prof. K.M. Kadish (USA), Prof. C. Rizzoli (Italy), and to Dr. E.M. Bauer, Dr. A.A. Gaberkorn, Dr. E.V. Kudrik. This work is part of a joint scientific project operative since 1999 between the University of Rome "La Sapienza" (Rome, Italy) and the University of Chemical Technology (Ivanovo, Russia). CE thanks the University of "La Sapienza" and the Italian MIUR (9903263473 and 2003038084) and PAS the Russian Foundation of Basic research (05-03-32921) for financial support.

References

[1] (a) G.T. Byrne, R.P. Linstead, A.W. Lowe, J. Chem. Soc. (1934) 1017;
(b) R.P. Linstead, A.W. Lowe, J. Chem. Soc. (1934) 1022;
(c) R.P. Linstead, J. Chem. Soc. (1953) 2873 (and references therein).
[2] C.C. Leznoff, A.B.P. Lever (Eds.), Phthalocyanines: Properties and Applications, vols. 1–4, VCH Publishers, Amsterdam, 1989–1996.
[3] K.M. Kadish, K.M. Smith, R. Guilard (Eds.), The Porphyrin Handbook, vols. 15–20, Academic Press, New York, 2003.
[4] S.L.J. Michel, B.M. Hoffman, S.M. Baum, A.G.M. Barrett, Progr. Inorg. Chem. 50 (2001) 473.
[5] R.P. Linstead, E.G. Noble, J.M. Wright, J. Chem. Soc. (1937) 911.
[6] J.A. Bilton, R.P. Linstead, J. Chem. Soc. (1937) 922.
[7] R.M. Christie, B.G. Freer, Dyes Pigm. 33 (1997) 107.
[8] M.J. Cook, A. Jafari-Fini, J. Mater. Chem. 7 (1997) 5.
[9] M.J. Cook, A. Jafari-Fini, Tetrahedron 56 (2000) 4085.
[10] V.N. Nemykin, A.E. Polshina, N. Kobayashi, Chem. Lett. (2000) 1236.
[11] S.V. Kudrevich, J.E. van Lier, Coord. Chem. Rev. 156 (1996) 163.
[12] P.A. Stuzhin, C. Ercolani, Porphyrazines with annulated heterocycles, in: K.M. Kadish, K.M. Smith, R. Guilard (Eds.), The Porphyrin Handbook, vol. 15, Academic Press, Amsterdam, 2003, pp. 263–364.
[13] C. Ercolani, P.A. Stuzhin, M.P. Donzello, E.M. Bauer, D. Cardarilli, R. Agostinetto, EP 9915533 A1 Chem. Abstr. 130 (1999) 261057.
[14] P.A. Stuzhin, E.M. Bauer, C. Ercolani, Inorg. Chem. 37 (1998) 1533.
[15] E.M. Bauer, D. Cardarilli, C. Ercolani, P.A. Stuzhin, U. Russo, Inorg. Chem. 38 (1999) 6414.
[16] E.M. Bauer, C. Ercolani, P. Galli, I.A. Popkova, P.A. Stuzhin, J. Porphyrins Phthalocyanines 3 (1999) 371.
[17] S. Angeloni, E.M. Bauer, C. Ercolani, I.A. Popkova, P.A. Stuzhin, J. Porphyrins Phthalocyanines 5 (2001) 881.
[18] (a) M.P. Donzello, C. Ercolani, P.A. Stuzhin, A. Chiesi-Villa, C. Rizzoli, Eur. J. Inorg. Chem. (1999) 2075;
(b) M.P. Donzello, D. Dini, G. D'Arcangelo, C. Ercolani, R. Zhan, Z. Ou, P.A. Stuzhin, K.M. Kadish, J. Am. Chem. Soc. 125 (2003) 14190.
[19] (a) M.P. Donzello, Z. Ou, F. Monacelli, G. Ricciardi, C. Rizzoli, C. Ercolani, K.M. Kadish, Inorg. Chem. 43 (2004) 8626;
(b) M.P. Donzello, Z. Ou, D. Dini, M. Meneghetti, C. Ercolani, K.M. Kadish, Inorg. Chem. 43 (2004) 8637;
(c) C. Bergami, M.P. Donzello, C. Ercolani, F. Monacelli, K.M. Kadish, C. Rizzoli, Inorg. Chem. 44 (2005) 9852.;
(d) C. Bergami, M.P. Donzello, F. Monacelli, C. Ercolani, K.M.Kadish, Inorg. Chem. 44 (2005) 9862.
[20] E.V. Kudrik, E.M. Bauer, C. Ercolani, P.A. Stuzhin, A. Chiesi-Villa, C. Rizzoli, Mend. Comm. (2001) 45.
[21] M.P. Donzello, C. Ercolani, A.A. Gaberkorn, E.V. Kudrik, M. Meneghetti, G. Marcolongo, C. Rizzoli, P.A. Stuzhin, Chem. Eur. J. 9 (2003) 4009.
[22] P.A. Stuzhin, E.A. Pozdysheva, O.V. Mal'chugina, I.A. Popkova, C. Ercolani, Chem. Heterocycl. Comp. 41 (2005) 246 (Translated from Khim. Geterotsiklicheskikh Soedinenii 41 (2005) 278–287).
[23] M.P. Donzello, R. Agostinetto, S.S. Ivanova, M. Fujimori, Y. Suzuki, H. Yoshikawa, J. Shen, K. Awaga, C. Ercolani, K.M. Kadish, P.A. Stuzhin, Inorg. Chem. 44 (2005) 8539.
[24] A.A. Gaberkorn, M.-P. Donzello, P.A. Stuzhin, Russ. J. Org. Chem. 42 (2006), in press.
[25] A.A. Gaberkorn, I.A. Popkova, P.A. Stuzhin, C. Ercolani Russ. J. Gen. Chem. (2006), in press.
[26] P.A. Stuzhin, C. Ercolani, in: Symposium Lecture ICPP3, J. Porphyrins Phthalocyanines 8 (2004) 495.
[27] M. Fujimori, Y. Suzuki, H. Yoshikawa, K. Awaga, Angew. Chem. 115 (2003) 6043.
[28] Y. Suzuki, M. Fujimori, H. Yoshikawa, K. Awaga, Chem. Eur. J. 10 (2004) 5158.
[29] S.M. Baum, A.A. Trabanco, A.G. Montalban, A.S. Micallef, C. Zhong, H.G. Meunier, K. Suhling, D. Phillips, A.J.P. White, D.J. Williams, A.G.M. Barrett, B.M. Hoffman, J. Org. Chem. 68 (2003) 1665.
[30] M. Zhao, C. Stern, A.G.M. Barrett, B.M. Hoffman, Angew. Chem. Int. Ed. 42 (2003) 462.
[31] M. Zhao, C. Zhong, C. Stern, A.G.M. Barrett, B.M. Hoffman, Inorg. Chem. 43 (2004) 3377.
[32] X. Zhou, A.-M. Ren, J.-K. Feng, Z. Shuai, J. Photochem. Photobiol. A: Chem. 172 (2005) 126.
[33] S. Angeloni, C. Ercolani, J. Porphyrins Phthalocyanines 4 (2000) 474.
[34] M.S. Rodriguez-Morgade, P.A. Stuzhin, J. Porphyrins Phthalocyanines 8 (2004) 1129.
[35] M.S. Fischer, D.H. Templeton, A. Zalkin, M. Calvin, J. Am. Chem. Soc. 93 (1971) 2622.
[36] S. Matzumoto, A. Endo, J. Mizuguchi, Z. Krystallogr. 215 (2000) 182.
[37] R.H. Hansn, C.E. Meloan, Inorg. Nucl. Chem. Lett. 7 (1971) 461.
[38] P.M. Solozhenkin, V.S. Tsveniashvili, E.V. Semenov, N.S. Khavtasi, Dokl. Akad. Nauk Tadzh. SSR 19 (1976) 38.
[39] A.S. Antsyshkina, O.A. Tokarskaya, V.Sh. Tsveniashvili, V.N. Ostrikova, L.Y. Ukhin, M.A. Porai-Koshits, A.D. Garnovskii, Koord. Khim. 15 (1989) 214.
[40] G.S. Papaefstathiou, A. Tsohos, C.P. Raptopoulou, A. Terzis, V. Psycharis, D. Gatteschi, S.P. Perlepes, Cryst. Growth Des. 1 (2001) 191.
[41] K. Skorda, G.S. Papaefstathiou, A. Vafiadis, A. Lithoxoidou, C.P. Raptopoulou, A. Terzis, V. Psycharis, E. Bakalbassis, V. Tangoulis, S.P. Perlepes, Inorg. Chim. Acta 326 (2001) 53.
[42] E.H. Moerkved, S.M. Neset, H. Kjoesen, G. Hvistendahl, F. Mo, Acta Chim. Scand. 48 (1994) 912.
[43] A.A. Gaberkorn, Y.B. Ivanova, O.V. Molodkina, M.-P. Donzello, I. Pimkov, C. Ercolani, V.B. Sheinin, P.A. Stuzhin, J. Porphyrins Phthalocyanines 8 (2004) 846.
[44] M. Zhao, C. Zhong, C. Stern, A.G.M. Barrett, B.M. Hoffman, J. Am. Chem. Soc. 127 (2005) 9769.
[45] C. Ercolani, E.V. Kudrik, S. Moraschi, I.A. Popkova, P.A. Stuzhin, First International Conference on Porphyrins and Phthalocyanines, Dijon, France, 2000, p. 575.
[46] I. Pimkov, I.A. Popkova, P.A. Stuzhin, Russ. J. Org. Chem., submitted for publication.
[47] S.W. Oliver, T.D. Smith, J. Chem. Soc. Perkin Trans. II (1987) 1579.
[48] K.J.M. Nolan, M. Hu, C.C. Leznoff, Synlett (1997) 593.
[49] J.M. Robertson, J. Chem. Soc. (1935) 615.
[50] R.B. Hammond, K.J. Roberts, R. Docherty, M. Edmonds, R. Gairns, J. Chem. Soc. Perkin Trans 2 (1996) 1527.
[51] P. Zugenmaier, T.L. Bluhm, Y. Deslandes, W.J. Orts, G.K. Hamer, J. Mater. Sci. 32 (1997) 5561.
[52] M.K. Engel, in: K.M. Kadish, K.M. Smith, R. Guilard (Eds.), The Porphyrin Handbook, vol. 20, Academic Press, Amsterdam, 2003.
[53] A. Bondi, J. Phys. Chem. 68 (1964) 441.

[54] S. Matsumoto, K. Matsuhama, J. Mizuguchi, Acta Cryst. C55 (1999) 132.
[55] (a) C.J. Brown, J. Chem. Soc. A (1968) 2844;
(b) C.J. Brown, Acta Cryst. A21 (1966) 137.
[56] J.F. Kirner, W. Dow, W.R. Scheidt, Inorg. Chem. 15 (1976) 1685.
[57] B.N. Figgis, E.S. Kucharski, P.A. Reynolds, J. Am. Chem. Soc. 111 (1989) 1683.
[58] W.R. Scheidt, W. Dow, J. Am. Chem. Soc. 99 (1977) 1101.
[59] K.J. Wynne, Inorg. Chem. 23 (1984) 4658.
[60] K. Yamasaki, O. Okada, K. Inami, K. Oka, M. Kotani, H. Yamada, J. Phys. Chem. B 101 (1997) 13.
[61] P.A. Stuzhin, J. Porphyrins Phthalocyanines 7 (2003) 813.
[62] A. Gieren, H. Betz, T. Huebner, V. Lamm, R. Neidlein, D. Droste, Z. Naturforsch. B39 (1984) 485.
[63] L.M. Weinstock, I. Shinkai, in: A.R. Katrizky (Ed.), Comprehensive Heterocyclic Chemistry. The Structure, Reactions, Synthesis and Uses of Heterocyclic Compounds, vol. 6, Pergamon Press, Oxford, 1984, pp. 513–543.
[64] A.M. Gyul'maev, I.V. Stankevich, Z.V. Todres, Khim. Geterotsikl. Soedin. (1973) 1473.
[65] M.H. Palmer, R.H. Findlay, J.N.A. Ridyard, A. Barrie, P. Swift, J. Mol. Struct. 39 (1977) 189.
[66] A. Bhattacharyya, A.A. Bhattacharyya, Indian J. Chem. 22B (1983) 802.
[67] T. Strassner, J. Fabian, J. Phys. Org. Chem. 10 (1997) 33.
[68] W. Gordy, J. Chem. Phys. 15 (1947) 305.
[69] P.A. Stuzhin, Diss. Dr. Chem. Sci. Ivanovo (2004) 383pp.
[70] M. Gouterman, G. Wagnier, L.C. Snyder, J. Mol. Spectr. 11 (1963) 108.
[71] A.B.P. Lever, Adv. Inorg. Chem. Radiochem. 7 (1965) 27.
[72] R.P. Linstead, M. Whalley, M. J. Chem. Soc. (1952) 4839.
[73] M.G. Gal'pern, E.A. Lukyanets, Zh. Obshch. Khim. 39 (1969) 2536.
[74] P.A. Stuzhin, I.S. Migalova, B.D. Berezin, A.V. Lubimov, Koord. Khim. 20 (1994) 444.
[75] K. Jerwin, F. Waagestian, Spectrochim. Acta 40A (1984) 159.
[76] M. Whalley, J. Chem. Soc. (1961) 866.
[77] A.A. Gaberkorn, Y.B. Ivanova, V.B. Sheinin, C. Ercolani, P.A. Stuzhin, in preparation.
[78] V.B. Sheinin, B.D. Berezin, O.G. Khelevina, P.A. Stuzhin, F.Y. Telegin, Zh. Org. Khim. 21 (1985) 1571.
[79] R. Stewart, T. Mattews, Can. J. Chem. 38 (1960) 607.
[80] H.H. Hyman, R.A. Garber, J. Am. Chem Soc. 81 (1959) 1847.
[81] B.D. Berezin, O.G. Khelevina, P.A. Stuzhin, Zh. Prikl. Spektrosk. 46 (1987) 809 [J. Appl. Spectrosc. 46 (1987) 510].
[82] P.A. Stuzhin, J. Porphyrins Phthalocyanines 3 (1999) 500 (and references therein).
[83] N.Y. Borovkov, A.S. Akopov, Zh. Fiz. Khim. 60 (1986) 750.
[84] A.A. Gaberkorn, Diss. Cand. Chem. Sci., Ivanovo State University of Chemical Technology (2004) 145pp.
[85] E. Benedetti, V. Bertini, Spectrochim. Acta 24A (1968) 57.
[86] A.A. El-Azhary, Acta Chem. Scand. 49 (1995) 11.
[87] K.N. Solovyov, L.L. Gladkov, A.A. Starukhin, S.F. Shkirman, Spektroskopija Porfirinov: Kolebatel'nye Sostojanija [Spectroscopyof Porphyrins: Vibrational States], Nauka i Tekhnika, Minsk, 1985, 416 pp.
[88] M.P. Sammes, J. Chem. Soc., Perkin Trans. 2 (1972) 160.
[89] L.L. Gladkov, S.F. Shkirman, V.K. Konstantinova, K.N. Solov'ev, Zh. Prikl. Spektr. 67 (2000) 551 [J. Appl. Spectrosc. 67 (2000) 755].
[90] K.V. Berezin, V.V. Nechaev, Zh. Prikl. Spektr. 70 (2003) 182 [J. Appl. Spectrosc. 70 (2003) 20].
[91] X. Zhang, Y. Zhang, J. Jiang, Vibr. Spectr. 33 (2003) 153.
[92] G. de la Torre, P. Vazques, F. Agullo-Lopez, T. Torres, J. Mater. Chem. 8 (1998) 1671.
[93] G. de la Torre, P. Vazquez, F. Agullo-Lopez, T. Torres, Chem. Rev. 104 (2004) 2723.
[94] F.A. Cotton, R. Francis, J. Am. Chem. Soc. 82 (1960) 2986.
[95] F. Calderazzo, D. Vitali, I. Collamati, G. Dessy, V. Fares, J. Chem. Soc., Dalton Trans. (1980) 1980.
[96] G. Rossi, M. Gardini, G. Pennesi, C. Ercolani, V.L. Goedken, J. Chem. Soc. (1989) 93.
[97] J. Janczak, R. Kubiak, Inorg. Chim. Acta 342 (2003) 64.
[98] J. Janczak, R. Kubiak, M. Sledz, H. Borrmann, Y. Grin, Polyhedron 22 (2003) 2689.
[99] D.W. Clack, J.R. Yandle, Inorg. Chem. 11 (1972) 1738.
[100] J. Mack, M.J. Stillman, in: K.M. Kadish, K.M. Smith, R. Guilard (Eds.), The Porphyrin Handbook, vol. 16, Academic Press, Amsterdam, 2003, p. 43.